PENALTY-BASED FINITE ELEMENT INTERFACE TECHNOLOGY FOR ANALYSIS OF HOMOGENEOUS AND COMPOSITE STRUCTURES

SUMMARY OF RESEARCH REPORT

For Project NAG-1-2213

Submitted to

NASA Langley Research Center

Submitted by

RONALD C. AVERILL

Department of Mechanical Engineering
Michigan State University
East Lansing, MI 48824-1226, U.S.A.

PENALTY-BASED FINITE ELEMENT INTERFACE TECHNOLOGY FOR ANALYSIS OF HOMOGENEOUS AND COMPOSITE STRUCTURES

RONALD C. AVERILL

Department of Mechanical Engineering, Michigan State University, East Lansing, MI 48824-1226, U.S.A.

Executive Summary

An effective and robust interface element technology able to connect independently modeled finite element subdomains has been developed. This method is based on the use of penalty constraints and allows coupling of finite element models whose nodes do not coincide along their common interface. Additionally, the present formulation leads to a computational approach that is very efficient and completely compatible with existing commercial software. A significant effort has been directed toward identifying those model characteristics (element geometric properties, material properties and loads) that most strongly affect the required penalty parameter, and subsequently to developing simple "formulae" for automatically calculating the proper penalty parameter for each interface constraint. This task is especially critical in composite materials and structures, where adjacent sub-regions may be composed of significantly different materials or laminates. This approach has been validated by investigating a variety of two-dimensional problems, including composite laminates.

1. INTRODUCTION

The ways in which analysis and design are performed have changed extensively during the past decade. Automated design algorithms are now plentiful and increasingly robust, and no longer are individual components of a structure designed in a vacuum. Facilitated in part by product data management (PDM) and product lifecycle management (PLM) software and internet-based data sharing, integrated design activities are now possible. Further, the speed and economy of modern computers have enabled engineers to perform many large scale analyses that were unheard of a decade ago. It is now common to analyze and simulate the response of entire aircraft, spacecraft, automobiles, ships, and other structural assemblies to a variety of complex and combined types of loading. The CPU time required to perform such analyses is very small compared to the time required for engineers to create the mathematical and computer models, and the latter effort is usually the most expensive component of a large scale analysis or simulation.

With model sharing and large scale analysis activities on the rise, it is becoming evident that improved technology for building computer models is needed. One issue that arises often is the need to perform a unified analysis of a structural assembly using sub-structural models created independently. These sub-structural models are frequently created by different engineers using different software and in different geographical locations, with little or no communication between the teams of engineers creating the models. As a result, these models are likely to be incompatible at their interfaces, making it very difficult to combine them for a unified analysis of the entire assembly.

Finite element interface technology has been developed during the past decade to

facilitate the joining of independently modeled substructures. Unconventional approaches have been employed to connect special elements based on analytical solutions to finite element models [1-2]. In [1] a near-field solution for a dynamically propagating crack at the interface of two dissimilar anisotropic elastic materials was successfully implemented into a hybrid-displacement finite element formulation. In [2] Lagrange multiplier terms are used to couple a special element, based on a stress analytical solution, to standard finite elements.

In order to take advantage of parallel computing, Farhat and colleagues [3-4] developed a domain decomposition approach for partitioning the spatial domain into a set of disconnected subdomains, each assigned to an individual processor. Lagrange multipliers were introduced to enforce compatibility at the interface nodes. In [5] non-conforming "mortar" elements are employed to connect incompatible subdomains using a conjugate gradient iterative technique in a domain decomposition scheme designed for parallel computers.

The finite element interface technology developed at NASA LaRC [6-10] and elsewhere [11] allows the connection of independently modeled substructures with incompatible discretization along the common boundary. This approach has matured to a point that it is now very effective. However, because the interface technology utilizes Lagrange multipliers to enforce the interface constraint conditions, the resulting system of equations is not positive-definite. Hence, state-of-the-art sparse solver technology cannot be utilized with the interface technology.

Recently, an alternative formulation for the finite element interface technology based on Lagrange multipliers has been developed [12]. The alternative approach recasts the interface element constraint equations in the form of multi-point constraints. This change allows an easier implementation of the formulation in a standard finite element code and alleviates the issues

related to the resulting non-positive definite system of equations. The method seems to provide reliable results, but the formulation of the interface method is still quite complicated.

A possible remedy for these shortcomings is to modify the current hybrid variational formulation of the interface element by enforcing the interface constraints via a penalty method as opposed to the current Lagrange multiplier approach. The primary consequences of this modification will be (i) a simple formulation that is easily implemented in commercial finite elements codes, (ii) a positive-definite and banded stiffness matrix and (iii) a reduced number of DOFs, since the Lagrange multiplier degrees of freedom (DOFs) will not be present. Thus, the proposed approach should greatly enhance the computational efficiency of the interface element technology.

From an accuracy point of view, the penalty method enforces the constraints only approximately, depending on the value of the penalty parameter chosen, while the Lagrange multiplier approach enforces the constraints exactly. The penalty method interface approach was recently attempted using a single global value of the penalty parameter to enforce all constraints [13]. This study demonstrated the validity and the effectiveness of the penalty approach in an interface element. However, there is need for specific guidelines regarding the selection of an appropriate value of the penalty parameter, especially when the substructures to be connected have different material and/or section stiffnesses.

There is a large body of literature related to the determination of an optimal value of the penalty parameter (see, e.g. [14-26]). However, there is no existing criterion for choosing the penalty parameter in the framework of the interface element under investigation. The determination of such a criterion is the primary thrust of the effort presented herein.

An effective and robust interface element technology has been developed using the

penalty method. A significant part of the effort has been directed toward identifying those model characteristics that most strongly affect the required penalty parameter, and subsequently to developing simple "formulae" for automatically calculating the proper penalty parameter for each interface constraint. The new approach has been validated through a wide variety of one and two-dimensional problems that have been investigated extensively from both an analytical and a computational point of view. Finally, the penalty based interface element technology has been implemented into an existing commercial code.

2. GENERAL DESCRIPTION OF THE INTERFACE ELEMENT

Consider two independently modeled subdomains Ω_1 and Ω_2 as shown in Figure 1(a) and 1(b), respectively, for a 2D and for a 3D geometry. The two substructures are connected to each other using an interface element acting like "glue" at the common interface. The interface element is discretized with a set of nodes that are independent of the nodes at the interface in subdomains Ω_1 and Ω_2. Both in the hybrid interface method and in the penalty method, the coupling terms associated to the interface element are arranged in the form of a "stiffness" matrix and assembled with the other finite element stiffness matrices as usual.

2.1 Hybrid Interface Method

The hybrid interface method [6-12] introduces two vectors of Lagrange multipliers λ_1 and λ_2 in the total potential energy (TPE) of the system to satisfy the displacement continuity conditions. Thus the TPE of the system assumes the form:

$$\pi = \pi_{\Omega_1} + \pi_{\Omega_2} + \int_S \lambda_1 (V - u_1) ds + \int_S \lambda_2 (V - u_2) ds \tag{1}$$

The nodal displacements of the sub-domain Ω_j are identified by q_j^o and q_j^i. The superscript o identifies the degrees of freedom (DOFs) that are not on the interfaces, while i denotes DOFs that are on the interfaces. The displacement field u_j of the sub-domain Ω_j is expressed in terms of the unknown nodal displacements q_j^i as:

$$u_j = N_j q_j^i \tag{2}$$

where N_j can be the matrices of linear Lagrange interpolation functions.

The displacement field V is approximated on the entire interface surface in terms of

unknown nodal displacements q_S as:

$$V = T\, q_s \tag{3}$$

where T is a matrix of cubic spline interpolation functions [27-29].

The first variation of π is taken with respect to all the DOFs and the vectors of Lagrange multipliers λ_1 and λ_2:

$$\delta\pi\big|_{q_1^o,\, q_1^i,\, q_S,\, q_2^o,\, q_2^i,\, \lambda_1,\, \lambda_2} = 0 \tag{4}$$

On the interface part of the subdomains the following equations result:

$$u_j = V, \quad \lambda_j = t_j, \quad \lambda_1 + \lambda_2 = 0 \qquad \text{for } j = 1,\, 2 \tag{5}$$

where t_j is the traction on the interface. These equations show that:

- Displacement continuity is enforced,
- λ_j are interface tractions,
- the total traction is zero on the interface.

The first variation of π yields the system of equations:

$$\begin{bmatrix} K_1^{ii} & K_1^{io} & 0 & 0 & 0 & M_1 & 0 \\ K_1^{oi} & K_1^{oo} & 0 & 0 & 0 & 0 & 0 \\ 0 & 0 & K_2^{ii} & K_2^{io} & 0 & 0 & M_2 \\ 0 & 0 & K_2^{oi} & K_2^{oo} & 0 & 0 & 0 \\ 0 & 0 & 0 & 0 & 0 & G_1 & G_2 \\ M_1^T & 0 & 0 & 0 & G_1^T & 0 & 0 \\ 0 & 0 & M_2^T & 0 & G_2^T & 0 & 0 \end{bmatrix} \begin{Bmatrix} q_1^i \\ q_1^o \\ q_2^i \\ q_2^o \\ q_s \\ \lambda_1 \\ \lambda_2 \end{Bmatrix} = \begin{Bmatrix} f_1^i \\ f_1^o \\ f_2^i \\ f_2^o \\ 0 \\ 0 \\ 0 \end{Bmatrix} \tag{6}$$

It can be seen that the resulting global stiffness matrix is sparse, symmetric, not banded and not positive definite. Inside $[K]$ the interface element is represented by the coupling terms M_j and G_j which augment the stiffness matrix of the subdomains.

A "stiffness" matrix and generalized vector of unknown displacements can be associated with the interface element, so that:

$$\begin{bmatrix} 0 & 0 & 0 & M_1 & 0 \\ 0 & 0 & 0 & 0 & M_2 \\ 0 & 0 & 0 & G_1 & G_2 \\ M_1^T & 0 & G_1^T & 0 & 0 \\ 0 & M_2^T & G_2^T & 0 & 0 \end{bmatrix} \begin{Bmatrix} q_1^i \\ q_2^i \\ q_s \\ \lambda_1 \\ \lambda_2 \end{Bmatrix} \tag{7}$$

2.2 *Penalty Hybrid Interface Method*

In the penalty hybrid interface method the displacement continuity constraint is imposed in a least squares sense through two vectors of penalty parameters γ_1 and γ_2. Thus the TPE of the system assumes the form:

$$\pi = \pi_{\Omega_1} + \pi_{\Omega_2} + \frac{1}{2}\gamma_1 \int_S (V - u_1)^2 \, ds + \frac{1}{2}\gamma_2 \int_S (V - u_2)^2 \, ds \tag{8}$$

The displacement fields u_j and V are approximated in a similar way as in the original hybrid interface method.

The first variation of π is taken with respect to all the DOFs, but not the vectors of penalty parameters γ_1 and γ_2, which are predetermined constants.

$$\delta\pi\big|_{q_1^e,\, q_1^i,\, q_s,\, q_2^e,\, q_2^i} = 0 \tag{9}$$

We now define:

$$G_j^{ii} = \gamma_j \int_S \left(N_j^T N_j \right) ds \tag{10}$$

$$G_j^{is} = \gamma_j \int_S \left(N_j^T T_j \right) ds \tag{11}$$

$$G_j^{si} = \left[G_j^{is} \right]^T \tag{12}$$

$$G_j^{ss} = \gamma_j \int_S \left(T_j^T T_j \right) ds \tag{13}$$

So the global system of equations of the penalty hybrid interface method assumes the following form:

$$\begin{bmatrix} K_1^{oo} & K_1^{oi} & 0 & 0 & 0 \\ K_1^{io} & K_1^{ii}+G_1^{ii} & -G_1^{is} & 0 & 0 \\ 0 & -G_1^{si} & G_1^{ss}+G_2^{ss} & -G_2^{si} & 0 \\ 0 & 0 & -G_2^{is} & K_2^{ii}+G_2^{ii} & K_2^{io} \\ 0 & 0 & 0 & K_2^{oi} & K_2^{oo} \end{bmatrix} \begin{Bmatrix} q_1^o \\ q_1^i \\ q_s \\ q_2^i \\ q_2^o \end{Bmatrix} = \begin{Bmatrix} f_1^o \\ f_1^i \\ 0 \\ f_2^i \\ f_2^o \end{Bmatrix} \tag{14}$$

This is a symmetric, banded and positive definite (after boundary conditions are imposed) global stiffness matrix. The "stiffness" matrix and generalized vector of unknown displacements associated with the interface element can be defined such that:

$$\begin{bmatrix} G_1^{ii} & -G_1^{is} & 0 \\ -G_1^{si} & G_1^{ss}+G_2^{ss} & -G_2^{si} \\ 0 & -G_2^{is} & G_2^{ii} \end{bmatrix} \begin{Bmatrix} q_1^i \\ q_s \\ q_2^i \end{Bmatrix} = \begin{Bmatrix} 0 \\ 0 \\ 0 \end{Bmatrix} \tag{15}$$

3. DETERMINATION OF THE PENALTY PARAMETERS

In the penalty method, the displacement continuity constraint is imposed through penalty parameters, a set of predetermined constants. The FE solution obtained using this method is approximate, with its accuracy depending on the value of the adopted penalty parameters. It is known that the penalty parameter should depend on the material and/or geometric properties of the two sub-regions being joined. Further, there is a relationship between the penalty parameter and the Lagrange multiplier that enforces a given constraint.

The Lagrange multiplier method imposes the continuity constraint exactly. Thus, the Lagrange multiplier method defines the upper limit to the accuracy of the penalty method. Knowledge of the correct solution facilitates relating the value of the penalty parameter to the geometrical and material properties of the model under consideration. In our pursuit of the proper penalty parameter values, a variety of one and two-dimensional problems have been studied with both the Lagrange multiplier method and the penalty method.

The types of finite elements that have been investigated are: conventionally formulated and reduced integrated Timoshenko beam elements, plane stress quadrilateral elements and plate elements based on the first order shear deformation theory (FSDT), or Mindlin plate theory. For each finite element formulation, different penalty parameters are associated to the various nodal DOFs. For example, the Timoshenko beam element has three independent nodal DOFs: the axial displacement u, the transverse displacement w and the rotation ψ. Thus, three different penalty parameters γ_u, γ_w and γ_ψ are employed to enforce the interface continuity constraints on the DOFs u, w and ψ. An independent choice of the penalty parameters is of fundamental importance since each degree of freedom can be related differently to the material and geometric properties

of the finite element model.

The methodology adopted in finding the relations will now be described. First the most common load cases for the FE type under consideration are applied separately to a simple model of one or two elements. For example, for the Timoshenko beam element the following load cases are considered: axial load, transversely distributed load, concentrated transverse load and concentrated moment applied at the tip. These loads are applied to two different models: a single beam element connected to a fixed point by one interface element (see Figure 2a), and two linear beam elements connected using an interface element and clamped at the tip (see Figure 2b).

The formulations and solutions are obtained using both the Lagrange multiplier method and the penalty method. The displacement solutions from the two methods are compared individually for each degree of freedom. The ratio between the two solutions is expressed in the form:

$$\frac{u^{penalty}}{u^{Lagrange}} = 1 + \frac{f}{\gamma} \tag{16}$$

where $f = f$(element geometric properties, material properties, and loads)

Once this simple expression has been identified, the penalty parameter γ is set equal to:

$$\gamma = \beta f \tag{17}$$

Then, the ratio between the solutions becomes independent of material and geometrical properties of the element:

$$\frac{u^{penalty}}{u^{Lagrange}} = 1 + \frac{1}{\beta} \tag{18}$$

The accuracy of the solution depends directly on the value assigned to the parameter β. For example, if β is equal to 1000, the penalty solution differs from that obtained by use of the

Lagrange multipliers by 0.1%. The degree of precision of the solution cannot be indefinitely increased, since round off amplification error would rise. However, once a reasonable compromise between constraint representation error and the round off error has been evaluated, a value of β can be identified that is able to produce the same level of accuracy for every combination of material and geometrical properties.

In some cases, however, the displacement solution related to a particular DOF depends on the penalty parameter used to enforce a different DOF. An example of this situation is represented by the following relations:

$$\frac{u_1^{penalty}}{u_1^{Lagrange}} = 1 + \frac{f_1}{\gamma_1} + \frac{f_2}{\gamma_2} \tag{19}$$

$$\frac{u_2^{penalty}}{u_2^{Lagrange}} = 1 + \frac{f_3}{\gamma_2} \tag{20}$$

where u_1 and u_2 are displacement solutions computed at the same node for two different DOFs, while f_1, f_2 and f_3 are independent functions of the model properties and the loads.

Two possible options are available in this situation. The first option is to choose $\gamma_1 = 2\beta f_1$ and $\gamma_2 = 2\beta f_2$ in order to obtain the desired simple relation between the solution ratio and β only for the DOF 1.

$$\frac{u_1^{penalty}}{u_1^{Lagrange}} = 1 + \frac{1}{2\beta} + \frac{1}{2\beta} = 1 + \frac{1}{\beta} \qquad \frac{u_2^{penalty}}{u_2^{Lagrange}} = 1 + \frac{f_3}{2\beta f_2} \tag{21}$$

The other option is to set $\gamma_1 = 2\beta f_1$ and $\gamma_2 = \beta f_3$, favoring a simple relation for the DOF 2.

$$\frac{u_1^{penalty}}{u_1^{Lagrange}} = 1 + \frac{1}{2\beta} + \frac{f_2}{\beta f_3} \qquad \frac{u_2^{penalty}}{u_2^{Lagrange}} = 1 + \frac{1}{\beta} \tag{22}$$

Clearly a conflict arises about the value of the penalty parameter γ_2. A reasonable way to

address this issue is to compare the two possible values for γ_2 and to choose the greater. Thus, the accuracy for one DOF is directly proportional to β as desired, and the precision of the other one should be slightly higher.

As discussed previously, one of the main objectives of this study is to establish an automatic choice of the optimal penalty parameter. The investigations of the ratio between the solutions based on Lagrange multipliers and the penalty method constitute the basis for pursuing this goal. Nevertheless, it should be underlined that an exact value of the penalty parameter is not required. Rather, a value that is of the right order of magnitude is sufficient. In fact, even in the most complex FE analysis, there exists a range of values for this parameter for which the numerical outcomes change very little. This range can equal as much as 12 orders of magnitude for simple analyses, but usually is not less than two orders of magnitude in most situations.

3.1 Computational Example – Beam Under Uniaxial Load

In order to limit the length and the complexity of the mathematical derivation, the example described here is one of the simplest available: the extension of a beam under a uniform load P applied at the tip. This case is analyzed using a single linear beam element connected to one fixed point V by a displacement continuity constraint, which is imposed through a Lagrange multiplier or a penalty parameter. The configuration of the geometry and the mesh is plotted in Figure 2a.

3.1.1 Lagrange Multiplier Method

The hybrid interface method introduces a Lagrange multiplier λ_1 in the total potential energy (TPE) of the system to satisfy the displacement continuity condition. Thus the TPE of the

system in this study assumes the following form.

$$\pi = \pi_1 + \lambda_1 \cdot (v - u_1) - r_1 \cdot v \tag{23}$$

where π_1 is the TPE of the bar; r_1 and v are, respectively, the reaction force and the displacement at point V. Expanding and simplifying:

$$\pi = \int_V \frac{1}{2}(\sigma_x \cdot \varepsilon_x) dV - \sum_{i=1}^{2} f_i \cdot u_i + \lambda_1 \cdot (v - u_1) - r_1 \cdot v \tag{24}$$

$$\pi = \frac{1}{2} \cdot \int_0^L EA\left(\frac{du}{dx}\right)^2 dx - \sum_{i=1}^{2} f_i \cdot u_i + \lambda_1 \cdot (v - u_1) - r_1 \cdot v \tag{25}$$

where E is the Young's modulus, A is the cross sectional area and f_i are the applied nodal forces. If the displacements are approximated linearly by:

$$u = \sum_{j=1}^{2} u_j N_j = u_1\left(1 - \frac{x}{L}\right) + u_2\left(\frac{x}{L}\right) \tag{26}$$

π takes the following form.

$$\pi = \frac{EA}{2} \cdot \int_0^L \left(\sum_i u_i \frac{dN_i}{dx}\right)\left(\sum_j u_j \frac{dN_j}{dx}\right) dx - P \cdot u_2 + \lambda_1 \cdot (v - u_1) - r_1 \cdot v \tag{27}$$

Setting to zero the first variation of π, taken with respect all the DOFs, produces the following equations.

$$\frac{\partial \pi}{\partial u_1} = EA \cdot \int_0^L \left(\frac{dN_1}{dx}\right)\left(\sum_j u_j \frac{dN_j}{dx}\right) dx - \lambda_1 = 0 \tag{28}$$

$$\frac{\partial \pi}{\partial u_2} = EA \cdot \int_0^L \left(\frac{dN_2}{dx}\right)\left(\sum_j u_j \frac{dN_j}{dx}\right) dx - P = 0 \tag{29}$$

$$\frac{\partial \pi}{\partial v} = \lambda_1 - r_1 = 0 \tag{30}$$

$$\frac{\partial \pi}{\partial \lambda_1} = v - u_1 = 0 \tag{31}$$

Thus, the resulting FE model is:

$$\begin{bmatrix} \frac{EA}{L} & -\frac{EA}{L} & 0 & -1 \\ -\frac{EA}{L} & \frac{EA}{L} & 0 & 0 \\ 0 & 0 & 0 & 1 \\ -1 & 0 & 1 & 0 \end{bmatrix} \begin{Bmatrix} u_1 \\ u_2 \\ v \\ \lambda_1 \end{Bmatrix} = \begin{Bmatrix} 0 \\ P \\ r_1 \\ 0 \end{Bmatrix} \tag{32}$$

Since V is fixed, $v = 0$, and the solution is found to be:

$$r_1 = \lambda_1 = -P \tag{33}$$

$$u_1 = v = 0 \tag{34}$$

$$u_2 = \frac{PL}{EA} \tag{35}$$

The solution provided by the hybrid interface method coincides with the exact theoretical one.

3.1.2 Penalty Method

In the penalty method the displacement continuity constraint is imposed through a penalty parameter γ_1. Therefore the TPE of the system takes the form:

$$\pi = \pi_1 + \frac{1}{2}\gamma_1 \cdot (v - u_1)^2 - r_1 \cdot v \tag{36}$$

$$\pi = \int_V \frac{1}{2}(\sigma_x \cdot \varepsilon_x)\, dV - \sum_{i=1}^{2} f_i \cdot u_i + \frac{1}{2}\gamma_1 \cdot (v - u_1)^2 - r_1 \cdot v \tag{37}$$

$$\pi = \frac{1}{2} \cdot \int_0^L EA\left(\frac{du}{dx}\right)^2 dx - \sum_{i=1}^{2} f_i \cdot u_i + \frac{1}{2}\gamma_1 \cdot (v - u_1)^2 - r_1 \cdot v \tag{38}$$

Approximating the displacements linearly:

$$\pi = \frac{EA}{2} \cdot \int_0^L \left(\sum_i u_i \frac{dN_i}{dx} \right) \left(\sum_j u_j \frac{dN_j}{dx} \right) dx - P \cdot u_2 + \frac{1}{2} \gamma_1 \cdot (v - u_1)^2 - r_1 \cdot v \tag{39}$$

The first variation of π in this case is taken with respect all the DOFs, but not the penalty parameter.

$$\frac{\partial \pi}{\partial u_1} = EA \cdot \int_0^L \left(\frac{dN_1}{dx} \right) \left(\sum_j u_j \frac{dN_j}{dx} \right) dx - \gamma_1 \cdot (v - u_1) = 0 \tag{40}$$

$$\frac{\partial \pi}{\partial u_2} = EA \cdot \int_0^L \left(\frac{dN_2}{dx} \right) \left(\sum_j u_j \frac{dN_j}{dx} \right) dx - P = 0 \tag{41}$$

$$\frac{\partial \pi}{\partial v} = \gamma_1 \cdot (v - u) - r_1 = 0 \tag{42}$$

The resulting FE model is:

$$\begin{bmatrix} \frac{EA}{L} + \gamma_1 & -\frac{EA}{L} & -\gamma_1 \\ -\frac{EA}{L} & \frac{EA}{L} & 0 \\ -\gamma_1 & 0 & \gamma_1 \end{bmatrix} \begin{Bmatrix} u_1 \\ u_2 \\ v \end{Bmatrix} = \begin{Bmatrix} 0 \\ P \\ r_1 \end{Bmatrix} \tag{43}$$

Solving the system of equations:

$$r_1 = -P \tag{44}$$

$$u_1 = \frac{P}{\gamma_1} \tag{45}$$

$$u_2 = \left(\frac{1}{\gamma_1} + \frac{L}{EA} \right) P \tag{46}$$

3.1.3 Comparison Between the Two Methods

When the penalty parameter approaches infinity, the penalty method solution tends to the one obtained using the Lagrange multiplier method.

$$\underset{\gamma_1 \to \infty}{Limit}\, u_1 = \underset{\gamma_1 \to \infty}{Limit} \frac{P}{\gamma_1} = 0 \tag{47}$$

$$\underset{\gamma_1 \to \infty}{Limit}\, u_2 = \underset{\gamma_1 \to \infty}{Limit} \left(\frac{1}{\gamma_1} + \frac{L}{EA} \right) P = \left(\frac{L}{EA} \right) P \tag{48}$$

Moreover, the constraint that has been enforced is:

$$C_1(u_1, u_2, v) = (v - u_1) \tag{49}$$

If we define $u_{1\gamma}, u_{2\gamma}, v_\gamma$ as the solutions derived from the penalty formulation, it is possible to verify the well-known relation between the Lagrange multiplier and the penalty parameter.

$$\lambda_1 = \gamma_1 \cdot C_1(u_{1\gamma}, u_{2\gamma}, v_\gamma) = \gamma_1 \cdot (v_\gamma - u_{1\gamma}) = \gamma_1 \cdot \left[0 - \frac{P}{\gamma_1} \right] = -P \tag{50}$$

3.1.4 Relation Between Penalty Parameter and Beam Properties

The exact displacement of the tip of the beam matches that from the Lagrange multiplier finite element formulation.

$$u_2^{exact} = \frac{L}{EA} P \tag{51}$$

The Penalty parameter solution $u_2^{penalty}$ differs from the exact one by the presence of an additional term (P/γ_1):

$$u_2^{penalty} = \left(\frac{1}{\gamma_1} + \frac{L}{EA} \right) P \tag{52}$$

The ratio $u_2^{penalty} / u_2^{exact}$ is evaluated in order to identify the relationship between the two solutions:

$$\frac{u_2^{penalty}}{u_2^{exact}} = \frac{\left(\frac{1}{\gamma_1} + \frac{L}{EA}\right)P}{\left(\frac{L}{EA}\right)P} = 1 + \frac{\left(\frac{EA}{L}\right)}{\gamma_1} \tag{53}$$

The penalty parameter γ_1 is now substituted by:

$$\gamma_1 = \beta \cdot \left(\frac{EA}{L}\right) \tag{54}$$

It follows that the ratio between the solutions becomes independent of material and geometrical properties of the beam.

$$\frac{u_2^{penalty}}{u_2^{exact}} = 1 + \frac{1}{\beta} \tag{55}$$

A similar procedure is followed for the two-dimensional and three dimensional problems of any kind. Details are omitted for brevity. But the final results of this investigation are presented in the appendix for selected element types.

A common approach is to set the penalty parameter equal to the largest diagonal term in the stiffness matrix multiplied by a factor 10^n, where n is a preselected integer value. For the simple example above, Eq. (54) yields an equivalent result. However, in general the approach developed here in yields expressions that are not directly proportional to coefficients in the stiffness matrix.

3.2 Automatic Round-Off Error Control

Due to finite precision in floating-point arithmetic used when the interface element stiffness matrix is numerically integrated, the stiffness coefficients are always approximated. However, in order to be imposed correctly (and to contribute no energy to the system), the

displacement continuity constraint $(V-u)$ requires the sum of the terms in every row of its stiffness matrix (15) to be zero. This condition usually cannot be achieved, due to the round-off error, and the resulting inaccuracy grows with the value of the penalty parameter. Precisely, the important measure is the ratio between the order of magnitude of the interface element stiffness matrix rows' imbalance and the element stiffness. If K_n is the stiffness associated to the n-th nodal DOF, it is sufficient to consider the ratio:

$$Q_n = \frac{ER_n}{K_n} \tag{56}$$

where ER_n is the unbalance in the interface element stiffness matrix row related to the DOF n.

$$ER_n = \sum_j K_{nj} \tag{57}$$

When the value of Q_n exceeds about $1 \cdot 10^{-4}$, errors in the solution may become appreciable. The discussed row imbalance is proportional to the value of the penalty parameter, $ER_n \propto \gamma$. It is also approximately true that:

$$ER_n \propto \gamma \propto \beta \cdot K_n \quad \Rightarrow \quad Q_n \propto \beta \tag{58}$$

Accordingly, an algorithm has been developed to control the round-off error. Its steps can be summarized as follows:

- Stiffness terms for every nodal DOF in the interface element are computed from known geometrical and material properties.
- For each row in the stiffness matrix:
    - The highest stiffness term is selected and assigned to a variable K
    - The row imbalance of the stiffness matrix is stored in a variable ER

- $Q = \dfrac{ER}{K}$ is evaluated

- The highest Q found is compared to a given constant value C. Typically $C = 1 \cdot 10^{-7}$ is used.

- If $Q > C$, the parameter β is reduced according to: $\beta^{new} = \dfrac{C}{Q} \cdot \beta$

- The interface element stiffness matrix is recalculated using the new value $\beta = \beta^{new}$.

This approach reduces the risk that round-off errors could adversely affect the solution. Thus, the initial value of β can be increased, in order to get a higher degree of accuracy, knowing that it will be automatically reduced if rounding errors don't allow that precision to be realized.

3.3 Implementation of the Model as an Abaqus User Element Subroutine

To test the behavior of the penalty method based "interface" element and the accuracy of the obtained relations for an automatic choice of the penalty parameters, the element has been implemented in the commercial finite element code ABAQUS as a User Element Subroutine (UEL) [30].

The UEL subroutine receives all the necessary information about geometry and material properties of the two connected meshes of finite elements from the input file. Then, the stiffness matrix of the interface element is built as previously defined:

$$\begin{bmatrix} G_1^{ii} & -G_1^{is} & 0 \\ -G_1^{si} & G_1^{ss} + G_2^{ss} & -G_2^{si} \\ 0 & -G_2^{is} & G_2^{ii} \end{bmatrix} \tag{60}$$

The appropriate values of penalty parameters for each constraint are assigned automatically inside the subroutine.

4. NUMERICAL RESULTS

4.1 Isotropic 2D Cantilever Beam with a Vertical Interface

A two dimensional cantilever beam is assumed to be composed of two domains. The domains are meshed independently and joined by one interface element. The geometrical and load configuration of the problem are represented in Figure 3. Others properties are: $P = 1$, $Q = 1$, $E_1 = E_2 = 1$ and $thickness = 1$.

Only one interface element is adopted in this simple case, since more would not improve the solution accuracy. This element is identified by the vertical interface that contains the three DOFs V_1, V_2 and V_3. In discretizing the two subdomains, four-noded bilinear plane stress elements are used. Two different load conditions are investigated: axial and bending loads. This problem may be considered a patch test for the element developed herein.

4.1.1 Axial Load

Under the condition of a uniformly distributed axial load applied at the free end of the beam, the interface element results are in agreement with the exact solution to the number of significant digits available. Results from two different beam discretizations are reported in Table 1.

It is important to study the stability of the solution obtained by the new method for various values of the nondimensionalized penalty parameter γ / E. For this test the automatic choice of the optimal parameter γ was temporarily disabled. Results are produced in graphical form in Figure 4. It can be observed that the solution is stable for a wide range of values of the nondimensionalized penalty parameter γ / E.

4.1.2 Bending Load

For the bending load case, a comparison is made to both the classical beam solution and a reference finite element solution. The coarse mesh of bilinear quadrilateral elements cannot exactly recover the classical solution. In Table 2 are results obtained from two different beam discretizations. The FE results, marked as Abaqus, are obtained from a traditional analysis using a compatible finite element model of the beam.

The stability of the solution obtained is tested also in this load case for various values of the nondimensionalized penalty parameter γ / E. Again the automatic choice of the optimal parameter γ was temporarily disabled. Results are produced in graphical form in Figure 5. The method proves very reliable and stable for bending loads.

4.2 Tension-Loaded Plate with a Central Circular Hole

A plate with a central circular hole is subjected to a uniform load at its edges. This well studied elasticity problem allows one to investigate the capability of the interface elements in performing global/local analysis. Geometrical and load configurations are plotted in Figure 6. The plate height and width are, respectively, $h = 100$ and $b = 200$; the radius of the hole is $r = 2.5$; the distance of the interface from the center of the hole is 5.

Taking advantage of symmetry, only one quarter of the plate is modeled. A fine mesh is applied in the area between the hole and the interface, while a much coarser mesh is adopted elsewhere. The complete finite element model is reported in Figure 7a. For a better view, the area near the hole is depicted in Figure 8a. The elements used to mesh the two domains are plane stress bilinear quadrilaterals, Abaqus CPS4. Five interface elements are employed along each segment of the interface for a total of 11 interface nodes.

Figures 9a and 10a demonstrate that only light discontinuities in the values of stresses at the interface are present. Horizontal and vertical displacements do not show any change in their values across the interface, as plotted in Figures 11a and 12a.

In order to compare the previous maps of stresses and displacements, a conventional FE model has been built with Abaqus. Figures 7b and 8b show the adopted mesh. Stresses σ_{11}, σ_{22} and displacements U_1 and U_2 are provided in Figures 9b to 12b. Comparing the maps of the displacements, it can be noticed that the interface elements do not introduce any discontinuities at the interface. The distribution of the stresses shows small differences, but they can still be considered sufficiently accurate.

The elasticity solution for an infinite plate with a central hole loaded in uniform tension predicts that the stress concentration factor, K_t, is equal to 3.0 at the upper edge of the hole. Moreover, it provides the equation for evaluating the change in σ_{11} along the line axis X_2. Using this expression, we computed the stress variation along X_2 for our geometrical configuration and compared this result with our FE models. Figure 13 graphs the exact elasticity solution against the penalty interface and the conventional FE ones. The results are all very close, validating the precision of the developed method.

4.3 Composite 2D Cantilever Beam with a Vertical Interface

A 2D composite cantilever beam made of five materials is considered. The geometrical and loading configurations are the same as for the cantilever beam analyzed previously (see Figure 14). The entire left domain of the beam is made of one isotropic material having a Young's modulus equal to 2.9E+7 MPa and Poisson's ratio 0.25. The right domain is composed

of four isotropic layers of equal thickness. They have all the same Poisson ratio 0.25, but the Young's modulus E varies. Starting from the bottom, the layerwise E takes the values: 1E+6 MPa, 1E+7 MPa, 5E+6 MPa and 1E+8 MPa. A conventional finite element model (10x4-10x4) has been used as a baseline to test the results from the penalty interface method.

Under these conditions the interface is expected to undergo abrupt changes of slope. An important property of the interface elements is the automatic choice of the penalty parameters. In fact, the interface elements can join the four different layers to the left domain with the dissimilar stiffness. This behavior can increase the accuracy of the results, avoiding the possible corrupting effect of an overestimated penalty parameter.

The results are shown for two possible interface discretizations: 1 interface element and 4 interface elements. Axial and vertical displacements at the free end of the beam under axial load are plotted in Figures 15 and 16. Similarly, deflections for transversal load case displacements at the free end of the beam are reported in Figures 17 and 18.

Displacements from the interface element model compare very well to those from the conventional finite element model. Only in the transversal load case, a single interface element appears to slightly overestimate the vertical displacements.

4.4 Clamped-Clamped Asymmetric Beam

In this section an asymmetric beam, clamped at both ends, is loaded with two concentrated loads applied at two different points of the mesh. This problem was studied in [4,13] to validate the proposed interface method. The geometry of the problem and the position of the two concentrated loads are shown in Figure 19.

The beam is meshed using two domains with different material properties. The ratio of

the Young's modulus in the domains a and b is 0.2. The domain a is discretized with an 8 by 8 mesh; two different meshes are adopted for the domain b. The mesh used for the conventional FE analysis is set to be 8 by 8, so that at the interface there is the same number of nodes. A different mesh is needed for discretizing domain b in order to test the interface model's capabilities. An 8 by 12 mesh has been chosen. The two forces, having the same magnitude F=1 but different directions, produce a complex state of deformation with strong stress concentrations at the interface that can challenge the interface element.

Figures 20 and 21 compare the deformed configuration, produced by a conventional FEM, with that obtained using a FEM with four interface elements at the interface. No visible differences can be observed.

The test is completed by a comparison between the in-plane displacements u and v along the interface as shown in Figures 22 and 23. The four interface elements connect two interfaces with a different number of nodes. Both displacement components are in satisfactory agreement with the conventional analysis.

4.5 Simply Supported Plate Under Sinusoidal Load

A simply supported plate is subjected to a transverse load distributed over the surface according to the following expression:

$$q = q_0 \sin\frac{\pi x}{a}\sin\frac{\pi y}{b} \tag{61}$$

In which q_0 represents the intensity of the load at the center of the plate. a and b are the plate dimensions, respectively, in the in-plane directions x and y.

We assume the plate to be square with equal side dimensions, $a = b = 2$. The value of q_0

is taken to be 1. Taking advantage of geometrical and loading symmetries, only a quarter of the plate is analyzed. As shown in Figure 24, a fine mesh is used for a square near the center, while the remaining surface adopts a coarse mesh. The four noded Abaqus shell element S4R is employed to mesh both domains. Two interface elements on each edge are used to connect the two domains. Others properties are: $E_1 = E_2 = 1e6$, $\nu = 0.25$ and thickness = 0.1. Figure 25 plots deformed and undeformed configurations of the plate as seen from the bottom.

A classical plate solution to this problem exists in the literature. In Figure 26, the transverse displacements w along x at $y = 1$ are reported. Even in the presence of a high gradient of deformation, the model behaves well. This further confirms our confidence that the developed method is both robust and accurate.

5. CONCLUSIONS

In the present work, an effective and robust interface element technology has been developed using the penalty method. This approach overcomes the numerical difficulties associated with the existing methods based on Lagrange multipliers. Additionally, the present formulation leads to a computational approach that is very efficient and completely compatible with existing commercial software. Significant effort has been directed toward identifying those model characteristics (element geometric properties, material properties and loads) that most strongly affect the required penalty parameter, and subsequently to developing simple "formulae" for automatically calculating the proper penalty parameter for each interface constraint. A wide variety of one and two-dimensional problems has been investigated analytically and computationally in order to correctly identify the analytical functional form of the penalty parameter for each constraint within many classes of problems.

The resulting interface element is particularly efficient for finite element modeling of composite structures. When the material properties vary across and/or along the interface, the present method is often much more accurate than adopting a unique value of the penalty parameter.

The present interface element has been implemented in the commercial finite element code ABAQUS as a User Element Subroutine (UEL), making it convenient to test the behavior and accuracy of the interface element for a wide range of problems. This approach has been validated by investigating a variety of two-dimensional problems, including composite laminates.

APPENDIX

The types of finite elements that have been investigated are: conventionally formulated and reduced integrated Timoshenko beam elements, plane stress quadrilateral elements and plate elements based on the first order shear deformation theory (FSDT), or Mindlin plate theory. For each finite element formulation, different relations between penalty parameters and model characteristics (element geometric properties, material properties and loads) have been found. Results of this investigation are briefly presented in this appendix.

Reduced integrated Timoshenko beam element

Consider the problem of two linear reduced integrated Timoshenko beams connected through an interface element. The interface node is identified as *i*, the last node of the first beam is identified as 1 and the first node of the second beam is identified as 2. The Timoshenko beam element has three independent nodal DOFs: the axial displacement u, the transverse displacement w and the rotation ψ. Thus, three different penalty parameters γ_u, γ_w and γ_ψ are employed to enforce the interface continuity constraints on the DOFs u, w and ψ. In Table A1 are defined the penalty parameters to be associated with each of the constraints.

Results obtained in our research lead us to affirm that the penalty parameters should be related to model characteristics as shown in Table A2. Where two values are present for the same DOF the bigger is chosen. Moreover, the subscript 1 and 2 marks, respectively, the material and geometrical properties belonging to the first and to the second beam.

Plane stress quadrilateral elements

As for the Timoshenko beam case, consider the problem of two plane stress quadrilateral

elements connected through an interface element. The generic node on the left of the interface is named 1, while the one on the right is named 2. Each node has two DOFs: the in-plane displacements u and v. Under conditions of axial load (load perpendicular to the interface surface), the following expression for the penalty parameter has been derived:

$$\gamma_k = \beta \cdot \left(\frac{E_k t_k}{a_k} \right) \qquad k = 1, 2$$

Where t_k and a_k are, respectively, the thickness and the width of the K^{th} element.

This expression is very simple, but still contains information that would be difficult to obtain, namely: the width of the element, a. Inside the UEL subroutine only the coordinates of the nodes on the interface are known. Thus, assuming good modeling practice in FE of using elements with aspect ratio close to unity, we choose to approximate the dimension in the direction perpendicular to the interface with the one parallel to it. According to the adopted symbols, the expression for γ_k becomes:

$$\gamma_k = \beta \cdot \left(\frac{E_k t_k}{b_k} \right)$$

This simplification strongly affects the expression obtained for the flexural load case (load parallel to the interface surface), which is modified in the following way:

$$\gamma_k = \left\{ \beta \cdot \left[\frac{\left(a_k^2 + 2b_k^2\right) E_k \, t_k}{4a_k \left(2a_k^2 + b_k^2\right)} \right] \right\} \xrightarrow{a_k = b_k} \gamma_k = \left\{ \beta \cdot \left[\frac{E_k \, t_k}{4b_k} \right] \right\}$$

A final step is required in order to obtain a single expression for an automatic evaluation of the penalty parameter. It consists in eliminating the scalar *4* from the denominator of the last expression for γ_k. This simplification is important since the interface could have any orientation, so it is better to not make any distinction between horizontal and vertical displacement DOFs. In

conclusion, only two penalty parameters are needed: γ_1 for both the DOFs u and v of the nodes on the left of the interface, γ_2 for the ones on the right of the interface.

$$\gamma_1 = \beta \cdot \left(\frac{E_1 t_1}{b_1} \right) \qquad \gamma_2 = \beta \cdot \left(\frac{E_2 t_2}{b_2} \right)$$

Plate elements

In plate elements each node has six DOFs: the in-plane displacements u and v, the transverse displacement w and the rotational DOFs (θ_x, θ_y, θ_z). The in-plane, transversal and rotational DOFs require different penalty parameters for optimal behavior. In particular: one, γ_u, is assigned to the in-plane DOFs (u, v), the second, γ_w, to the transverse DOF w and the third, γ_θ, is shared by all the rotational DOFs (θ_x, θ_y, θ_z). The constraints are associated to the expression for computing the penalty parameters as in Table A3.

Results obtained using the presented method have been simplified as for the plane stress quadrilateral element by approximating the element dimension in the direction perpendicular to the interface with the one parallel to it. The simplified relations are shown in Table A4.

5.1 REFERENCES

[1] Aminpour, M.A. and K. A. Hosapple. "Finite element solutions for propagating interface crack with singularity elements", *Engineering Fracture Mechanics*, Vol. 39, No. 3, 1991, pp. 451-468.

[2] Z. Jinping and A. Huizu. "Stress analysis around holes in orthotropic plates by subregion mixed finite element method", *Computers & Structures*, Vol. 41, No. 1, 1991, pp. 105-108.

[3] Farhat and F. X. Roux. "A method of finite element tearing and interconnecting and its parallel solution algorithm", *Journal for Numerical Methods in Engineering*, Vol. 32, 1991, pp. 1205-1227.

[4] C. Farhat and M. Gerardin. "Using a reduced number of Lagrange multipliers for assembling parallel incomplete field finite element approximations", *Computer Methods In Applied Mechanics And Engineering*, Vol. 97, 1992, pp. 333-354.

[5] Y. Maday, C. Mavriplis and A. Patera. "Non-conforming mortar element methods: Application to spectral discretizations", *NASA CR-181729*, ICASE Report No. 88-59, 1988.

[6] J.B. Ransom, S.L. McCleary and M. A. Aminpour. "A New Interface Element for Connecting Independently Modeled Substructures", *AIAA Paper*, Number 93-1503, 1993.

[7] J.M. Housner, M. A. Aminpour, C.G. Davila, J.E. Schiermeier, W.F. Stroud, Ransom, J.B., and R.E. Gillian. "An Interface Element for Global/Local and Substructuring Analysis", presented at the *MSC World Users' Conference*, Los Angeles, CA, May 8-12, 1995.

[8] M. A. Aminpour, J. B. Ransom, and S. L. McCleary. "A Coupled Analysis Method for Structures with Independently Modeled Finite Element Subdomains", *International Journal for Numerical Methods in Engineering*, Vol. 38, 1995, pp. 3695-3718.

[9] J.B. Ransom. "Interface Technology for Geometrically Nonlinear Analysis of Multiple Connected Subdomains", *AIAA* Paper No. 97-1298, 1997.

[10] M. A. Aminpour and T. Krishnamurthy. "A Two-Dimensional Interface Element for Multi-Domain Analysis of Independently Modeled Three-Dimensional Finite Element Meshes", *AIAA* paper no. 97-1297, 1997, pp. 1853-1861.

[11] M. A. Aminpour, T. Krishnamurthy and T. D. Fadale. "Coupling of Independently Modeled Three-Dimensional Finite Element Meshes with Arbitrary Shape Interface Boundaries", *AIAA* paper no. 98-2060, 1998, pp. 1853-186 1.

[12] M. A. Aminpour, Stephane Pageau and Youngwon Shin. "An Alternative Method for the Interface Modeling Technology", *AIAA* paper no. 2000-1352, 2000, pp. 1-13.

[13] Maenghyo Cho and Won Bae Kim. "A Coupled Finite Element Analysis of Independently Modeled Substructures by Penalty Frame Method", *AIAA* paper no. 98-2061, 1998, pp. 3025-3032.

[14] Carlos A. Felippa. "Error Analysis of Penalty Function Techniques for Constraint Definition in Linear Algebraic System", *International Journal for Numerical Methods in Engineering*, Vol. 11, 1977, pp. 709-728.

[15] Carlos A. Felippa. "Interactive Procedures for Improving Penalty Function Solutions of Algebraic System", *International Journal for Numerical Methods in Engineering*, Vol. 12, 1978, pp. 821-836.

[16] Carlos A. Felippa. "Penalty-Function Interactive Procedures for Mixed Finite Elements Formulation", *International Journal for Numerical Methods in Engineering*, Vol. 22, 1986, pp. 267-279.

[17] G. Prathap. "Locking, Rank and Singularity of Penalty-Linked Stiffness Matrix and Consistency of Strain-Field", *Computers & Structures*, Vol. 52, No. 1, 1994, pp. 35-39.

[18] Ahmed K. Noor and Jeanne M. Peters. "Penalty Finite Element Models for Nonlinear Dynamic Analysis", *AIAA Journal*, Vol. 24, No. 2, 1986, pp. 312-320.

[19] Ahmed K. Noor, M. Asce and Jeanne M. Peters. "Penalty Finite Element Formulation for Curved Elastica", *Journal of Eng. Mechanics*, Vol. 110, No. 5, 1984, pp. 694-712.

[20] E. Haugeneder. "A New Penalty Function Element For Thin Shell Analysis", *International Journal for Numerical Methods in Engineering*, Vol. 18, 1982, pp. 845-861.

[21] Ted Belytschko and Mark 0. Neal. "Contact-Impact by the Pinball Algorithm With Penalty And Lagrangian Methods", *International Journal for Numerical Methods in Engineering*, Vol. 31, 1991, pp. 547-572.

[22] G. F. Carey and R. Krishnan. "Convergence Of Iterative Methods In Penalty Finite Element Approximation Of The Navier-Stokes Equations", *Computer Methods In Applied Mechanics And Engineering*, Vol. 60, 1991, pp. 1-29.

[23] J. N. Reddy. "On The Accuracy And Existence Of Solutions To Primitive Variable Models Of Viscous Incompressible Fluids", *Int. J. Engineering Sci.*, Vol. 16, 1978, pp. 921-929.

[24] Henry Bertin and Hiroyuki Ozoe. "Technique For Rapid Convergence Of The Penalty Finite-Element Method With A Modified Galerkin Scheme And Its Application To Natural Convection", *Numerical Heat Transfer*, vol. 10, 1986, pp. 311-325.

[25] E-M. Salonen. "An Iterative Penalty Function Method In Structural Analysis", *International Journal for Numerical Methods in Engineering*, Vol. 10, 1976, pp. 413-421.

[26] R. Codina, M. Cervera And E. Orate. "A Penalty Finite Element Method For Non-Newtonian Creeping Flows", *International Journal for Numerical Methods in Engineering*, Vol. 36, 1993, pp. 1395-1412.

[27] A. W. Al-Khafaji and J. R. Tooley. "Numerical Methods in Engineering Practice", *HRW Series in Mechanical Engineering*, 1986.

[28] M. L. James, G.M. Smith and J. C. Wolford. "Applied Numerical Methods for Digital Computation", *Harper & Row*, 1985.

[29] Arthur Sard and Sol Weintraub. "A Book of Splines", *Wiley*, 1971.

[30] Abaqus Manuals, Hibbit, Karlsson & Sorensen Inc., 1999.

Table 1. *Tip axial displacement numerical results for beam extension.*

	Mesh	*Solution*
Abaqus	20x8	**4.000**
Abaqus with interface Element	10x8 Left / 10x2 Right 10x8 Left / 10x4 Right	**4.000** **4.000**
Classical	-	**4.000**

Table 2. *Tip deflection numerical results for beam flexure.*

	Mesh	*Solution*
Abaqus	20x2 20x4 20x8	**258.800** **260.000** **260.400**
Abaqus with interface Element	10x8 Left / 10x2 Right 10x8 Left / 10x4 Right 10x8 10x8 Left / 10x8 Right	**259.500** **261.100** **260.400**
Classical	-	**265.6**

Table A1. *Penalty parameters associated with each of the constraints enforced in the Timoshenko beam element.*

Penalty parameter	Constraint enforced
γ_{u1}	$(u_i - u_1)$
γ_{w1}	$(w_i - w_1)$
$\gamma_{\psi 1}$	$(\Psi_i - \Psi_1)$
γ_{u2}	$(u_i - u_2)$
γ_{w2}	$(w_i - w_2)$
$\gamma_{\psi 2}$	$(\Psi_i - \Psi_2)$

Table A2. *Expression for computing the penalty parameters in a Timoshenko beam element.*

	Axial load	Moment applied at the tip	Transverse load applied at the tip	Transversely Distributed Load
γ_{u1}	$\beta \cdot \left(\frac{E_1 A_1}{L_1} \right)$	-	-	-
γ_{w1}	-	-	$\beta \cdot \frac{2}{\left(\frac{L_1^3}{4E_1 I_1} + \frac{L_1}{k_1 A_1 G_1} \right)}$	$\beta \cdot \frac{2L_1}{\left(\frac{L_1^4}{8E_1 I_1} + \frac{L_1^2}{2k_1 A_1 G_1} \right)}$
$\gamma_{\psi 1}$	-	$\beta \cdot \frac{2E_1 I_1}{L_1}$	$\beta \cdot \frac{2L_1^2}{\left(\frac{L_1^3}{4E_1 I_1} + \frac{L_1}{k_1 A_1 G_1} \right)}$ or $\beta \cdot \frac{E_1 I_1}{L_1}$	$\beta \cdot \frac{2L_1^3}{\left(\frac{L_1^4}{4E_1 I_1} + \frac{L_1^2}{k_1 A_1 G_1} \right)}$ or $\beta \cdot \frac{2E_1 I_1}{L_1}$
γ_{u2}	$\beta \cdot \left(\frac{E_2 A_2}{L_2} \right)$	-	-	-
γ_{w2}	-	-	$\beta \cdot \frac{2}{\left(\frac{L_2^3}{4E_2 I_2} + \frac{L_2}{k_2 A_2 G_2} \right)}$	$\beta \cdot \frac{2L_2}{\left(\frac{L_2^4}{8E_2 I_2} + \frac{L_2^2}{2k_2 A_2 G_2} \right)}$
$\gamma_{\psi 2}$	-	$\beta \cdot \frac{2E_2 I_2}{L_2}$	$\beta \cdot \frac{2L_2^2}{\left(\frac{L_2^3}{4E_2 I_2} + \frac{L_2}{k_2 A_2 G_2} \right)}$ or $\beta \cdot \frac{E_2 I_2}{L_2}$	$\beta \cdot \frac{2L_2^3}{\left(\frac{L_2^4}{4E_2 I_2} + \frac{L_2^2}{k_2 A_2 G_2} \right)}$ or $\beta \cdot \frac{2E_2 I_2}{L_2}$

Table A3. ***Penalty parameters associated with each of the constraints enforced in a Mindlin plate element.***

Penalty parameter	Constraint enforced
γ_{u1}	$(u_i - u_1)$
γ_{v1}	$(v_i - v_1)$
γ_{w1}	$(w_i - w_1)$
$\gamma_{\theta 1}$	$(\theta_i - \theta_1)$
γ_{u2}	$(u_i - u_2)$
γ_{v2}	$(v_i - v_2)$
γ_{w2}	$(w_i - w_2)$
$\gamma_{\theta 2}$	$(\theta_i - \theta_1)$

Table A4. ***Expression for computing the penalty parameters in a Mindlin plate element.***

	All kind of loads
γ_{u1}	$\beta \cdot \left(\frac{E_1 t_1}{b_1} \right)$
γ_{v1}	$\beta \cdot \left(\frac{E_1 t_1}{b_1} \right)$
γ_{w1}	$\beta \cdot \frac{2}{\left(\frac{4b_1^3}{E_1 t_1^3} + \frac{1}{k_1 G_1 t_1} \right)}$
$\gamma_{\theta 1}$	$\beta \cdot \frac{2b_1^2}{\left(\frac{4b_1^3}{E_1 t_1^3} + \frac{1}{k_1 G_1 t_1} \right)}$ or $\beta \cdot \frac{t_1^3 E_1}{6}$
γ_{u2}	$\beta \cdot \left(\frac{E_2 t_2}{b_2} \right)$
γ_{v2}	$\beta \cdot \left(\frac{E_2 t_2}{b_2} \right)$
γ_{w2}	$\beta \cdot \frac{2}{\left(\frac{4b_2^3}{E_2 t_2^3} + \frac{1}{k_2 G_2 t_2} \right)}$
$\gamma_{\theta 2}$	$\beta \cdot \frac{2b_2^2}{\left(\frac{4b_2^3}{E_2 t_2^3} + \frac{1}{k_2 G_2 t_2} \right)}$ or $\beta \cdot \frac{t_2^3 E_2}{6}$

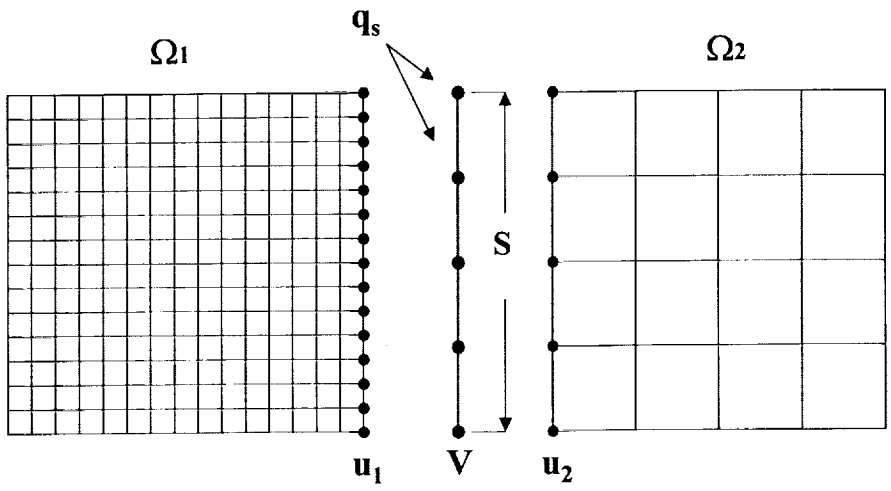

(a)

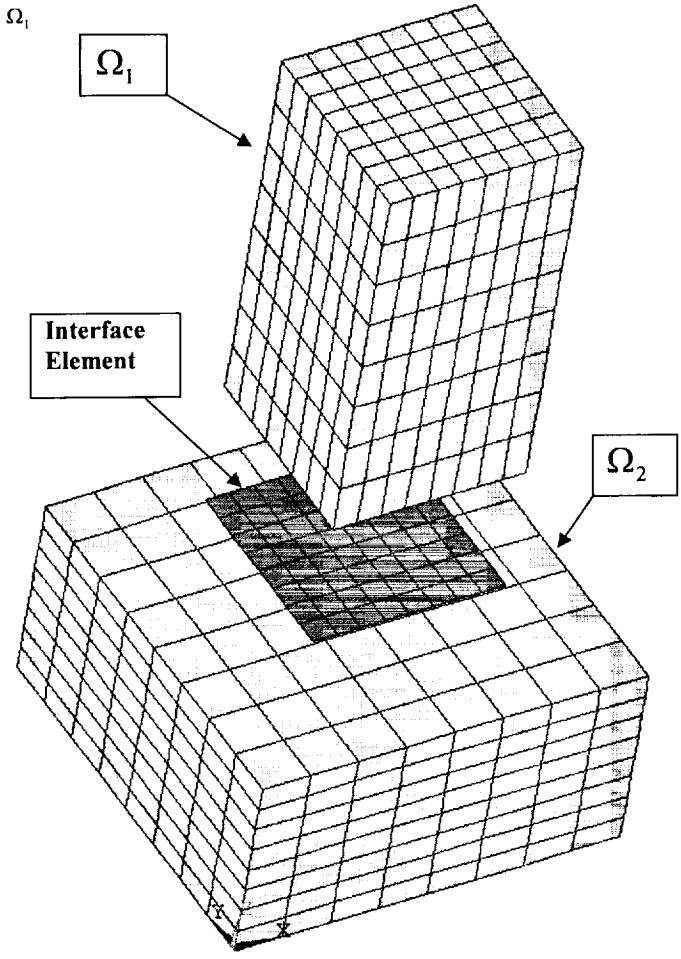

(b)

Figure 1. (a) 2D and (b) 3D Interface element configurations.

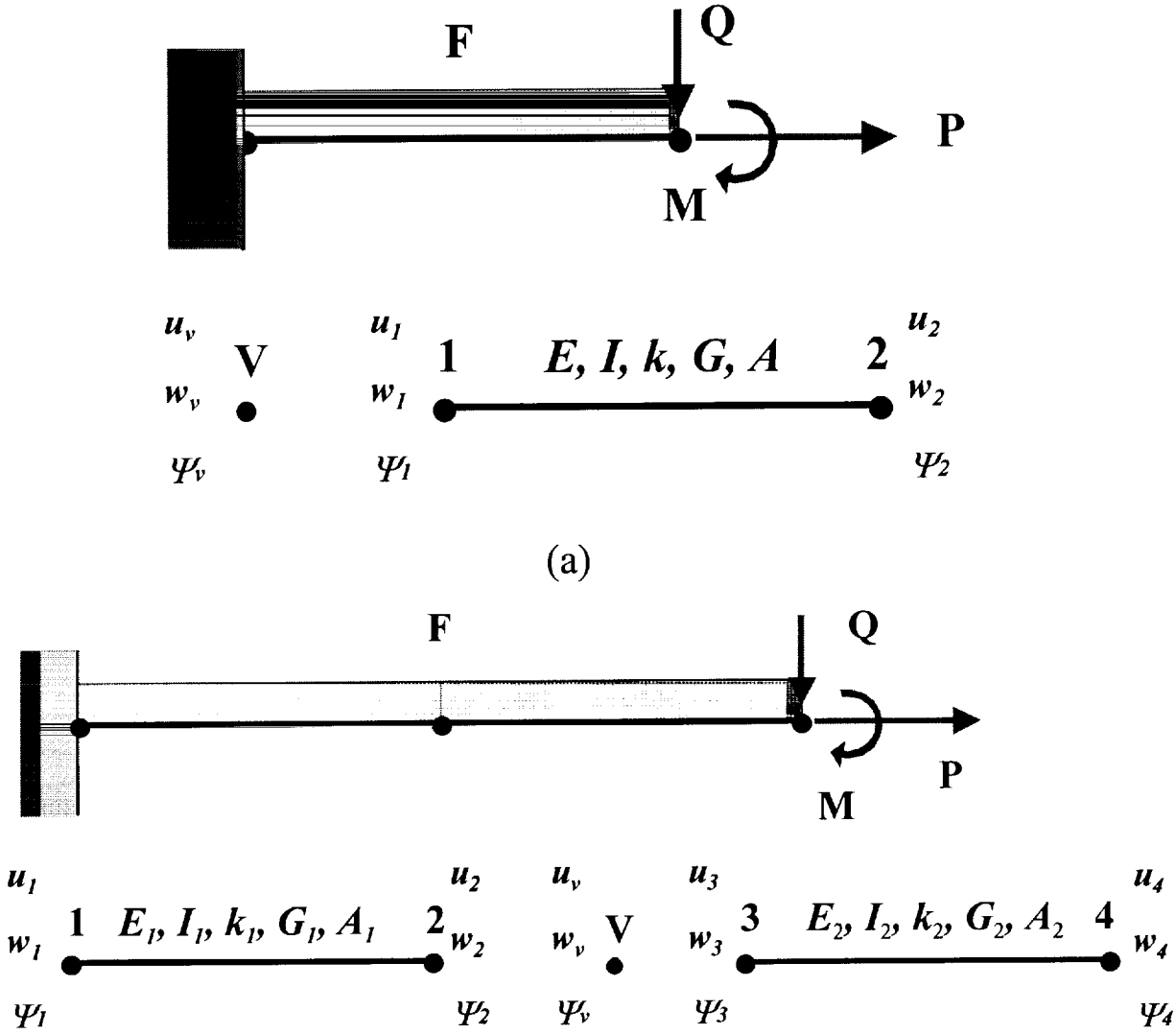

Figure 2. (a) Beam element connected to a fixed point V by one interface element; (b) two linear beam elements connected in V using an interface element and clamped at one tip.

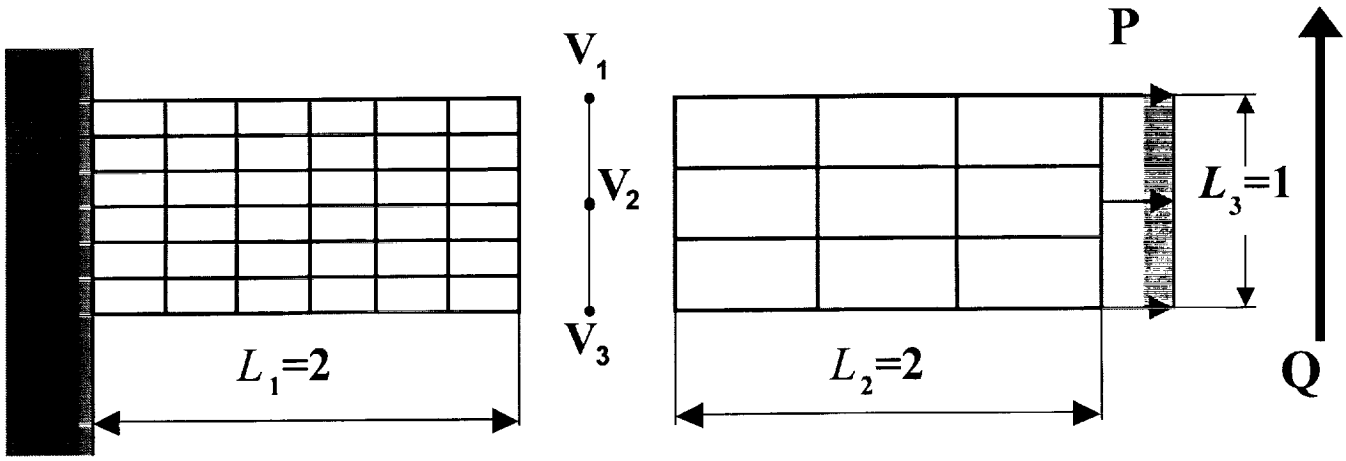

Figure 3. 2D- Cantilever beam with vertical interface.

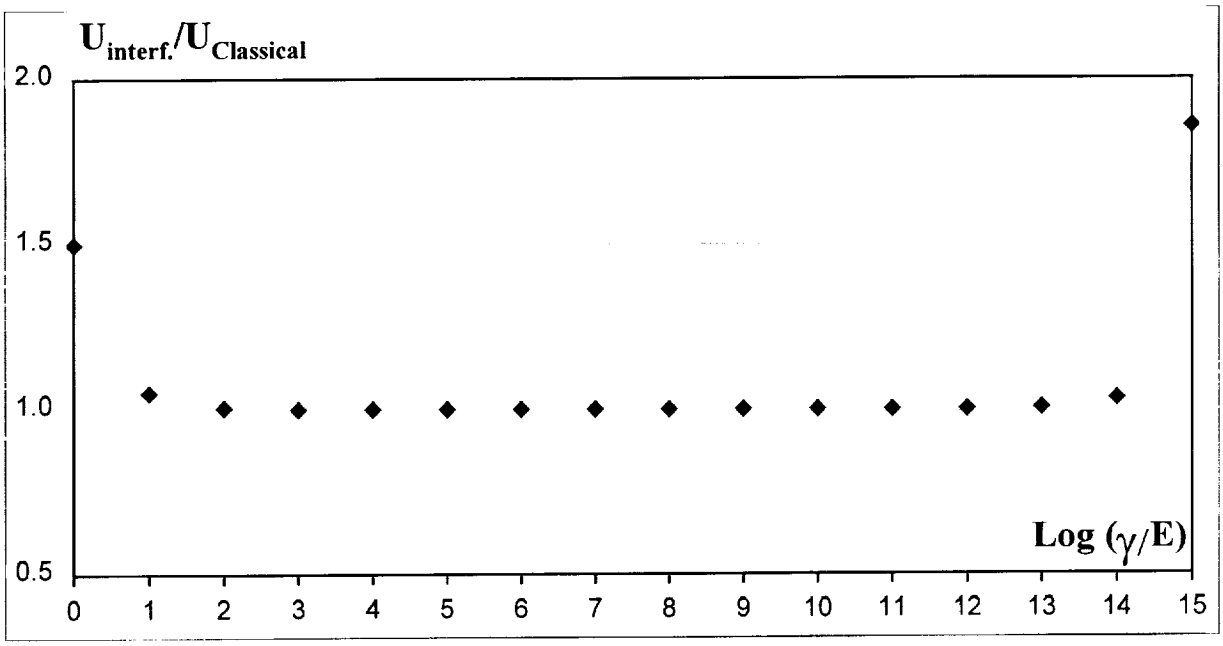

Figure 4. Stability of the solution for different values of γ- axial load.

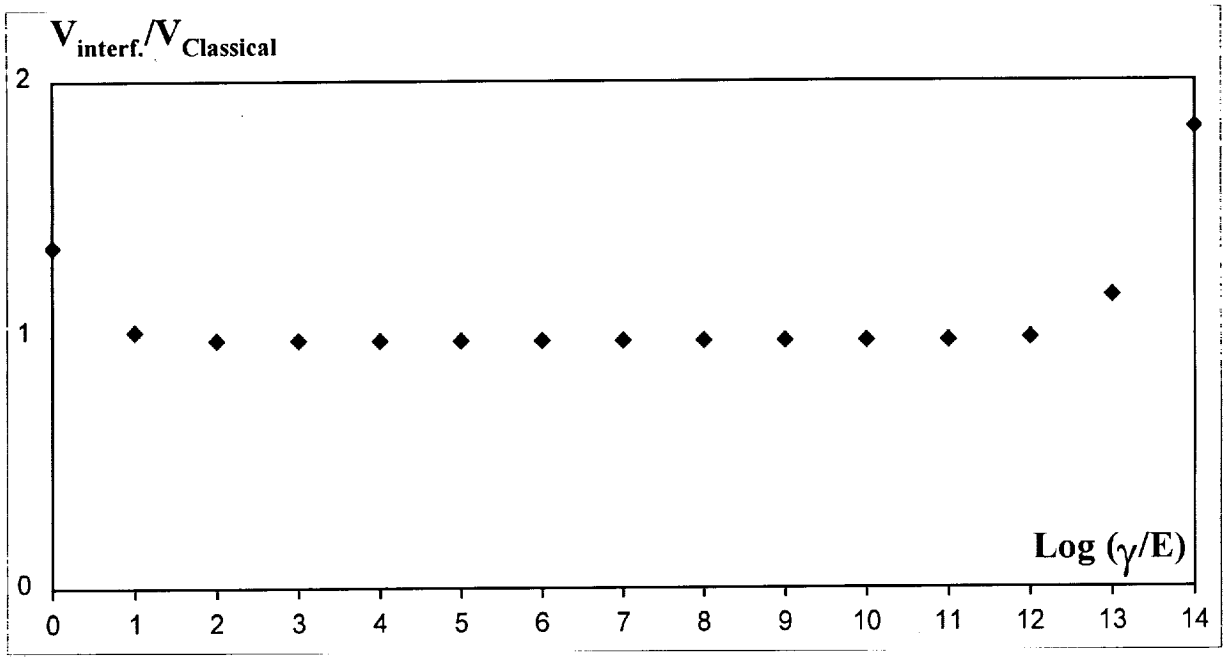

Figure 5. Stability of the solution for different values of γ - bending load.

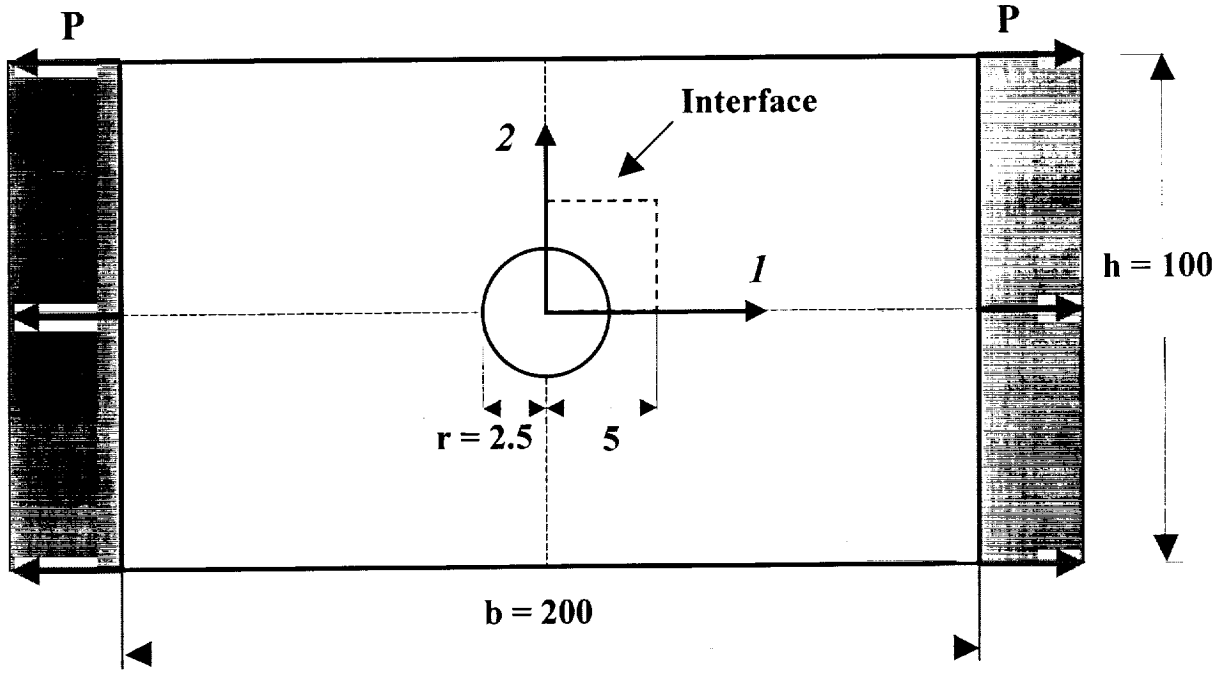

Figure 6. Tension-loaded plate with a central circular hole (not to scale).

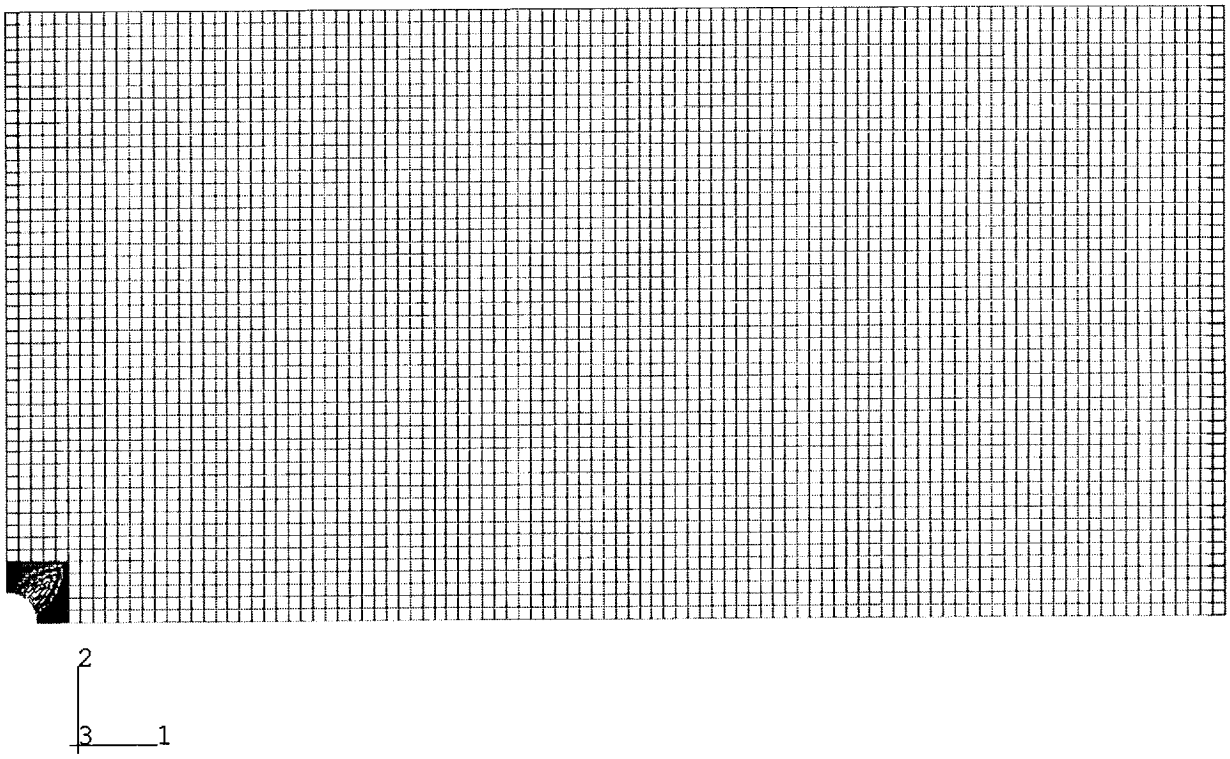

(a)

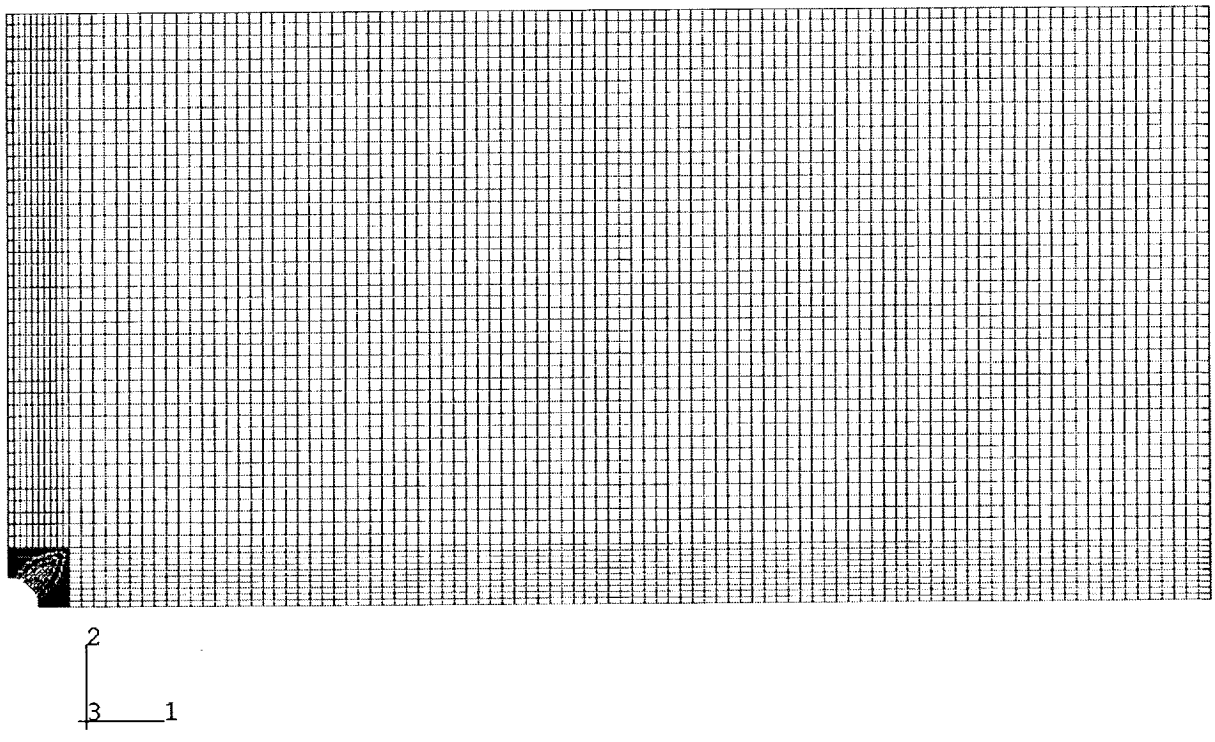

(b)

Figure 7. (a) Interface element and (b) conventional FE mesh.

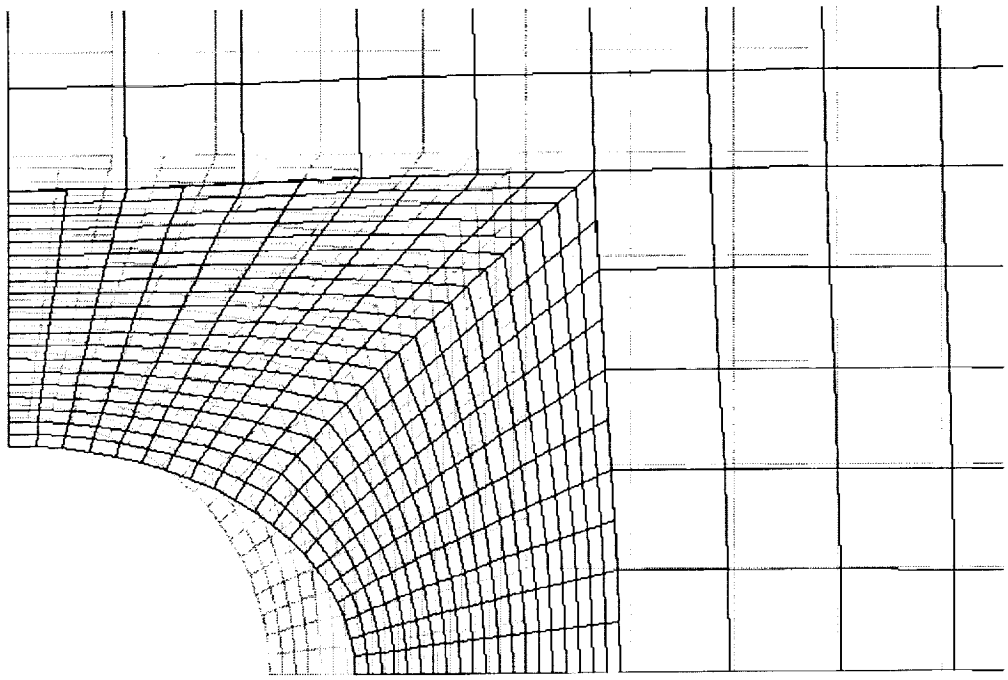

(a)

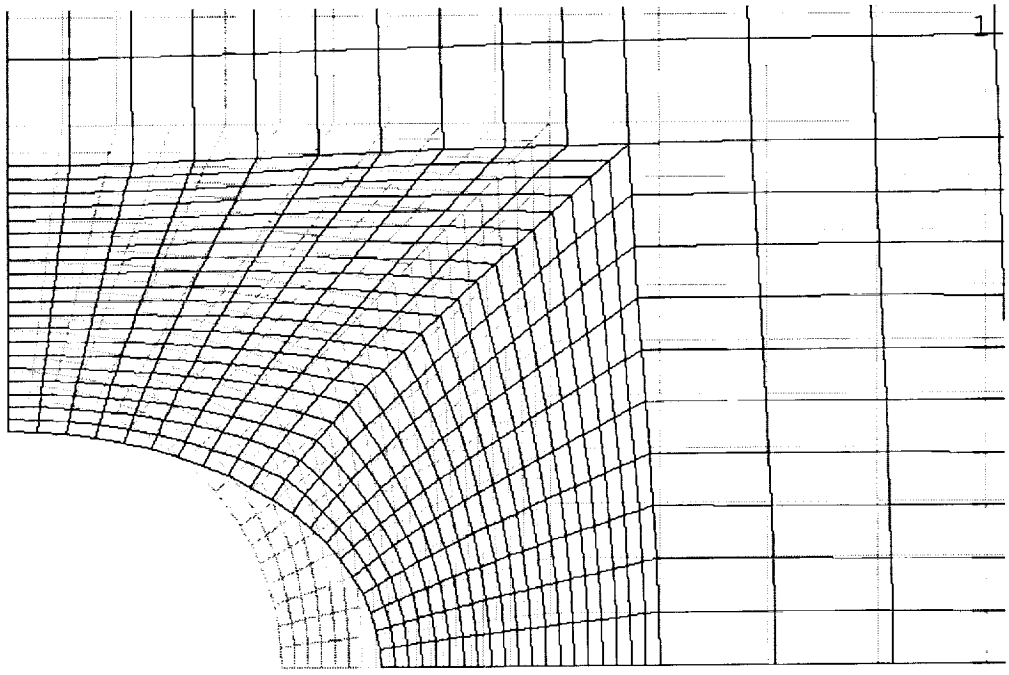

(b)

Figure 8. (a) Interface element and (b) conventional FE mesh - zoom of the deformed configuration.

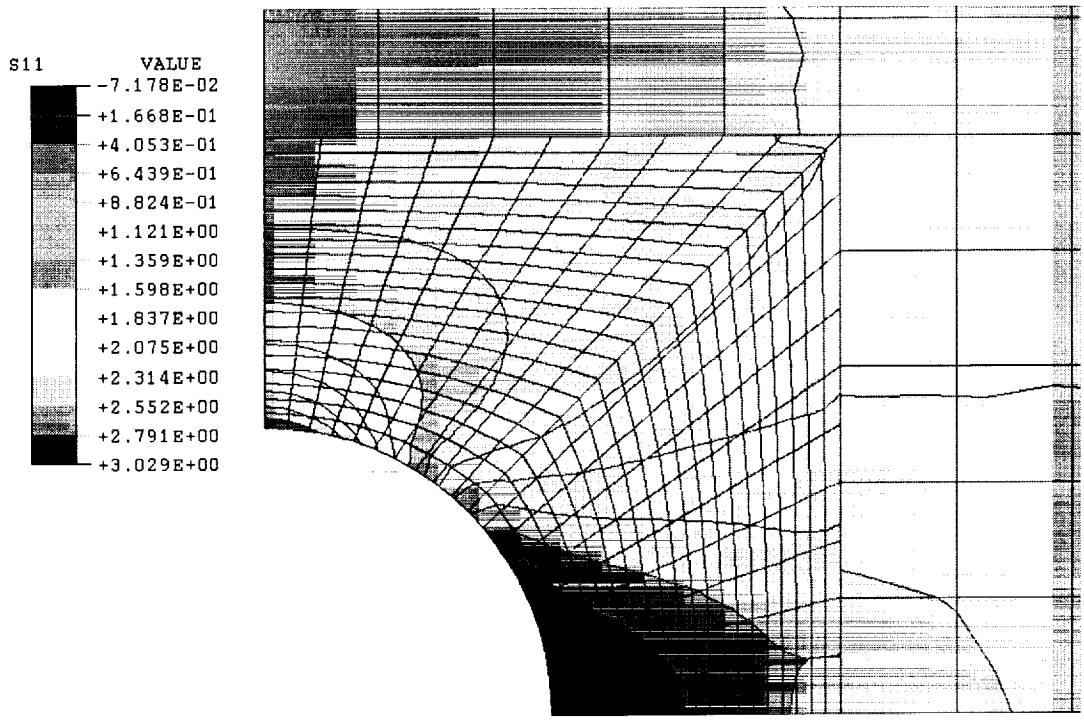

(a)

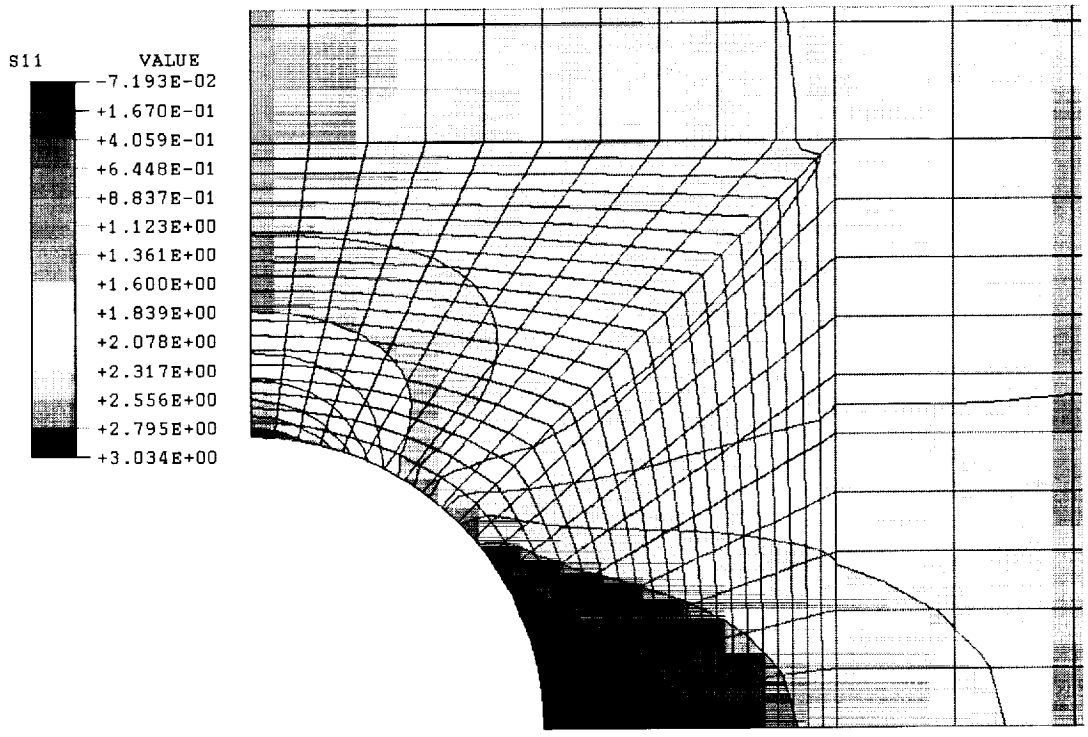

(b)

Figure 9. (a) Interface element and (b) conventional FE solution - stress distribution in the direction 1 (σ_{11}).

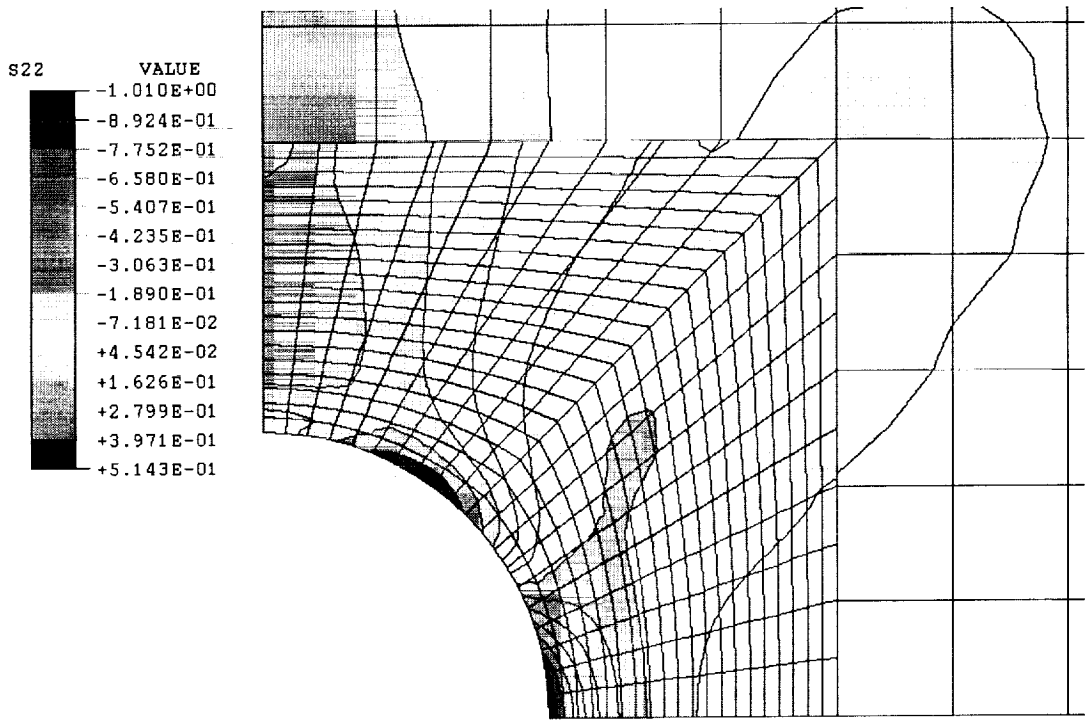

(a)

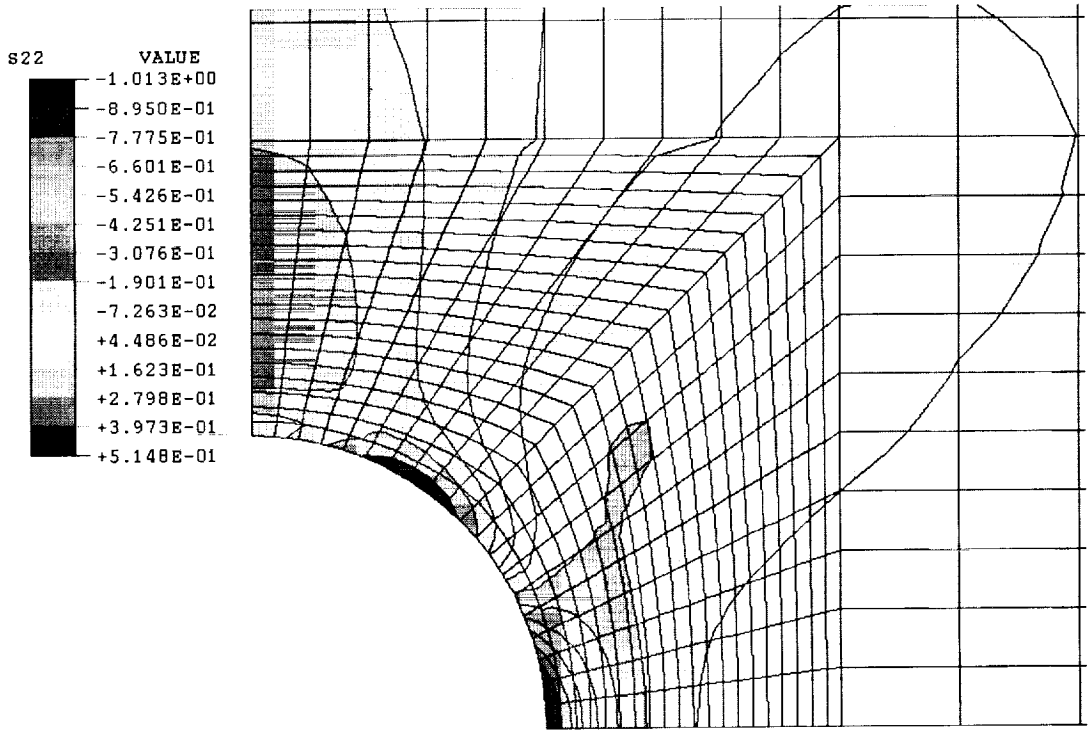

(b)

Figure 10. (a) Interface element and (b) conventional FE solution - stress distribution in the direction 2 (σ_{22}).

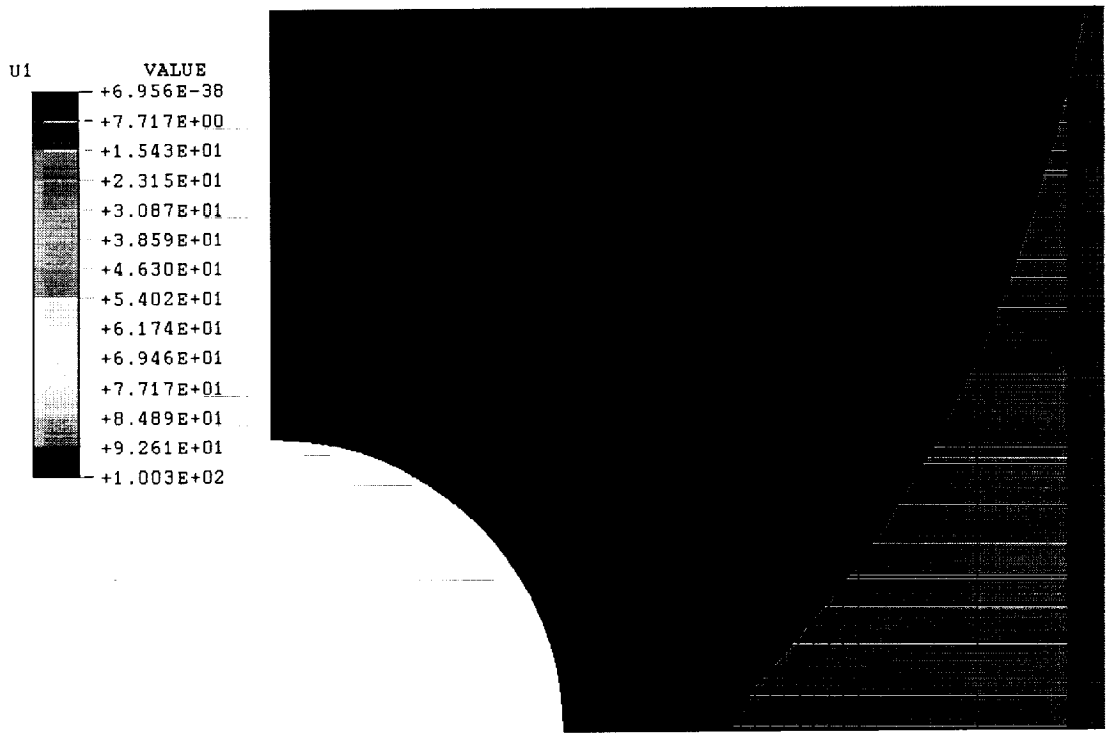

(a)

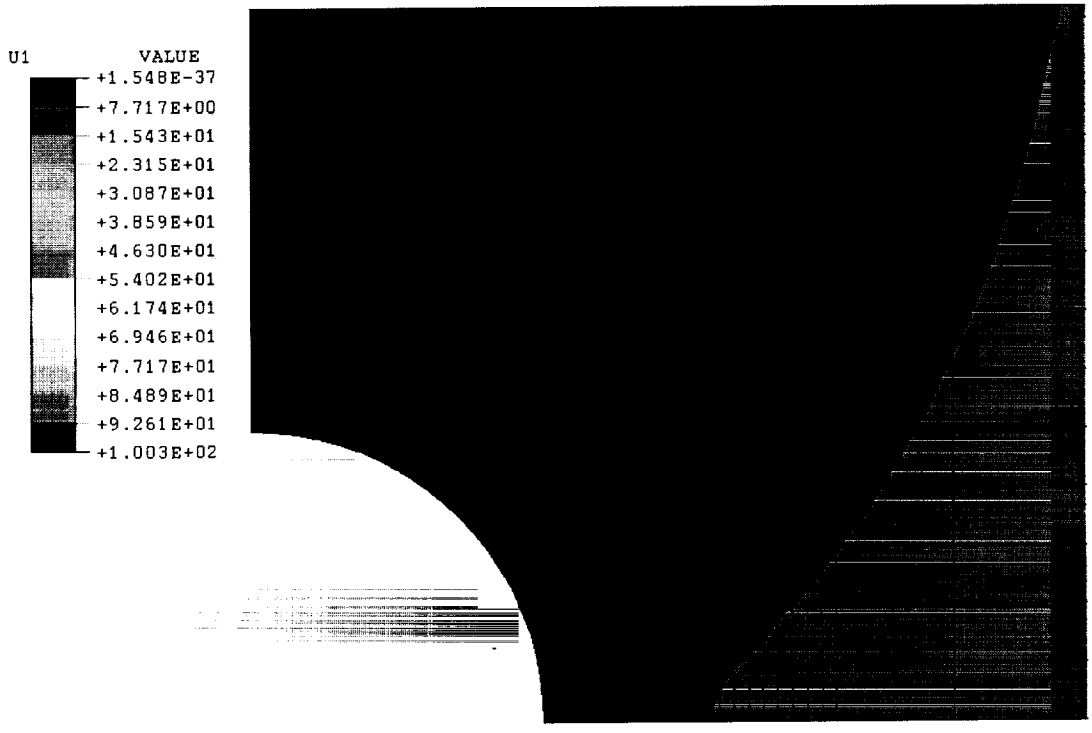

(b)

Figure 11. (a) Interface element and (b) conventional FE solution - horizontal displacement distribution (U_1).

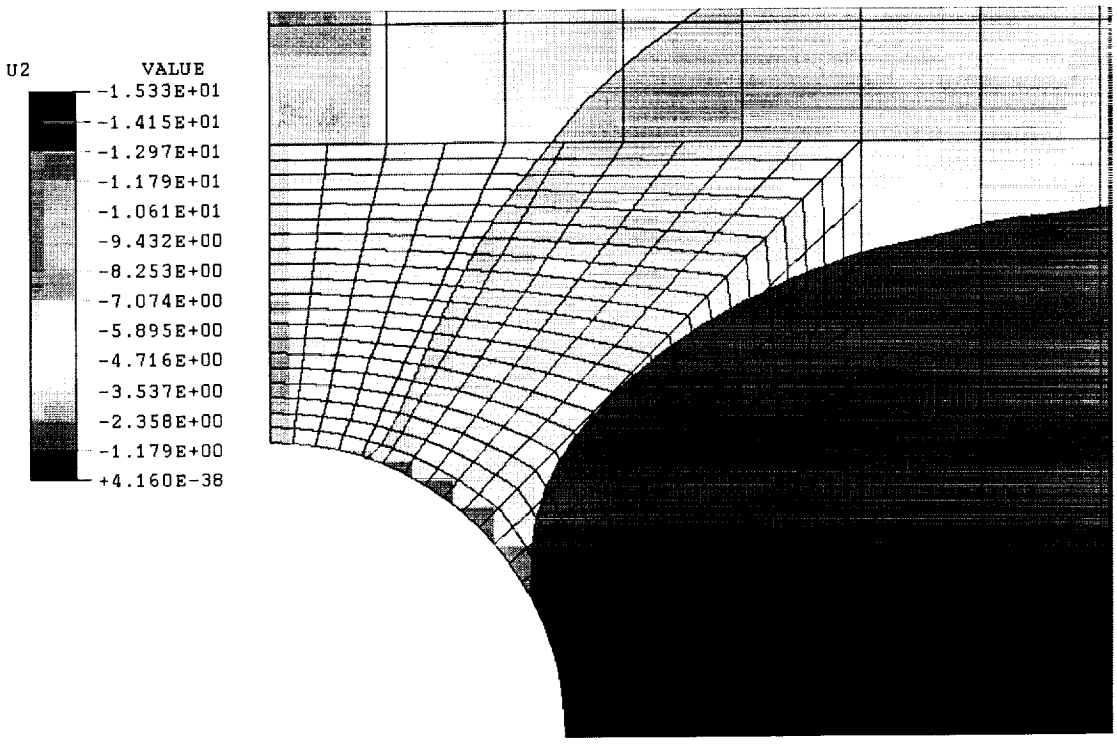

(a)

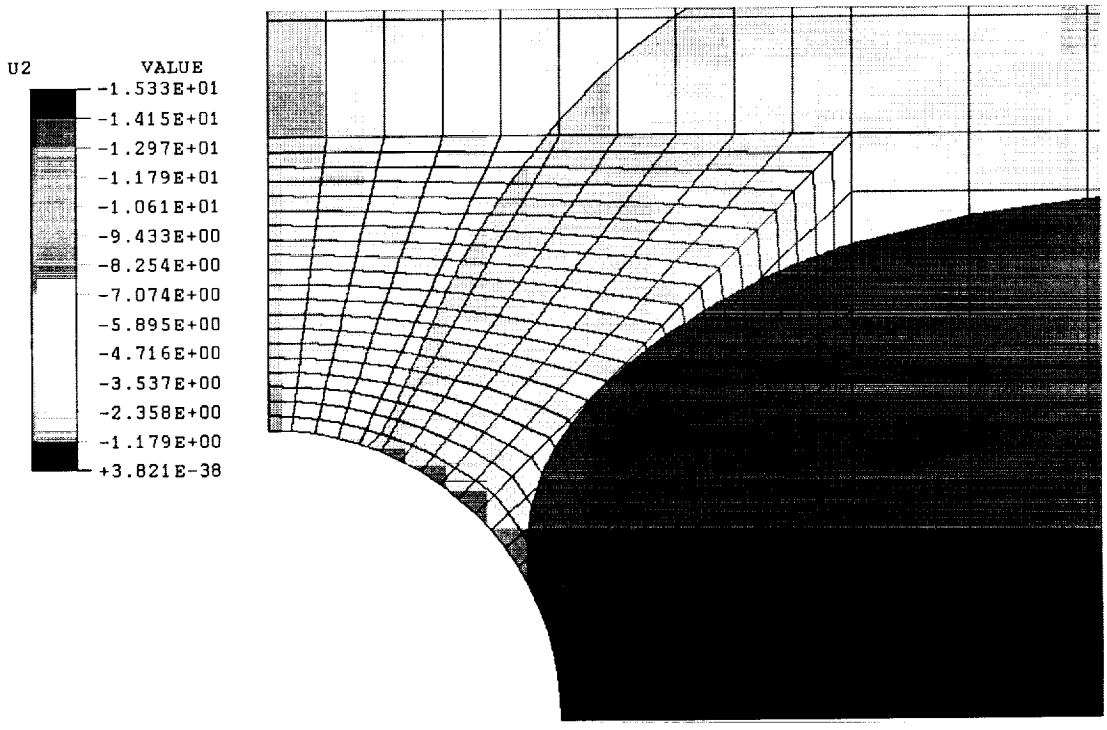

(b)

Figure 12. (a) Interface element and (b) conventional FE solution -

vertical displacement distribution (U_2).

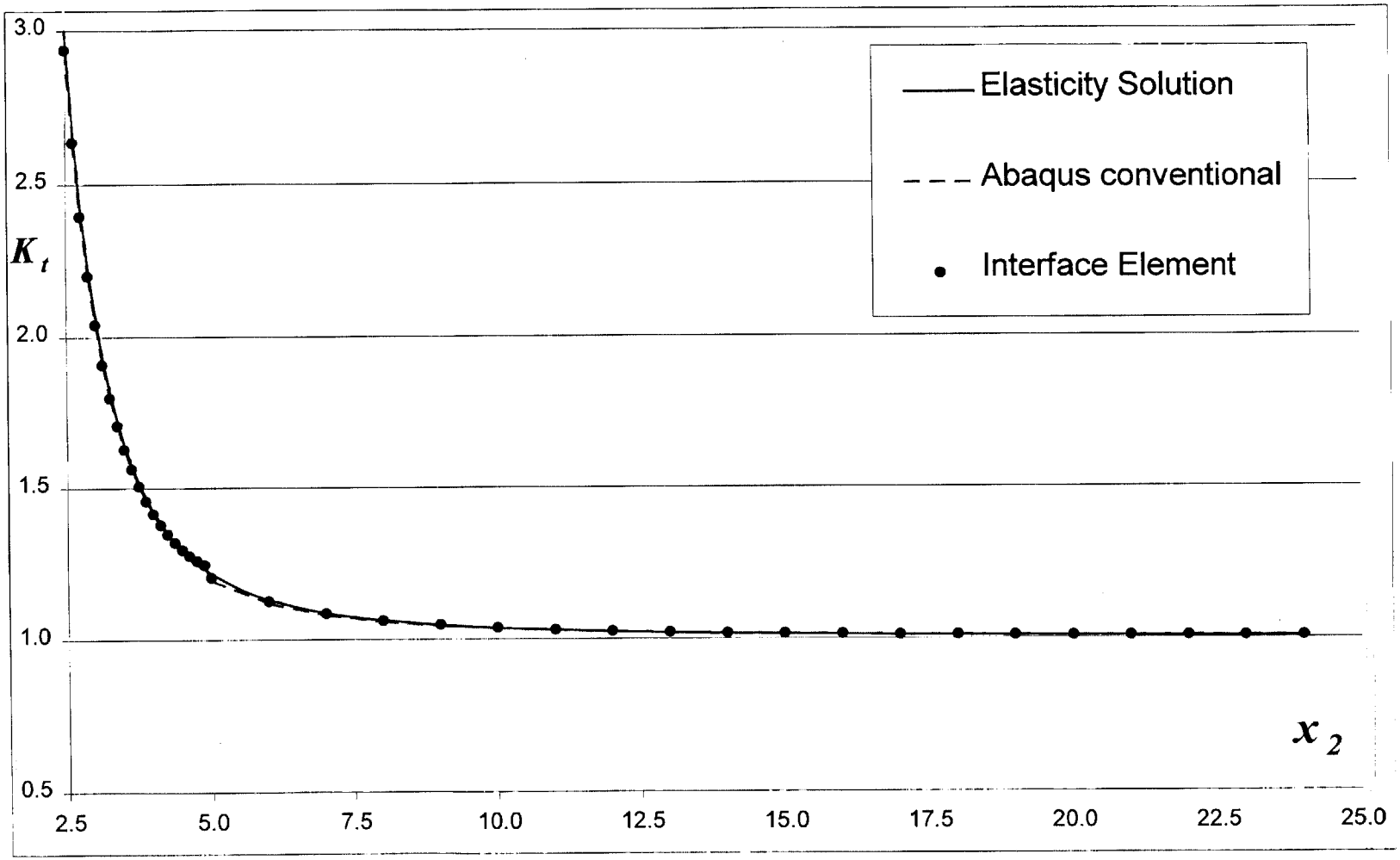

Figure 13. Stress concentration factor along the axis 2.

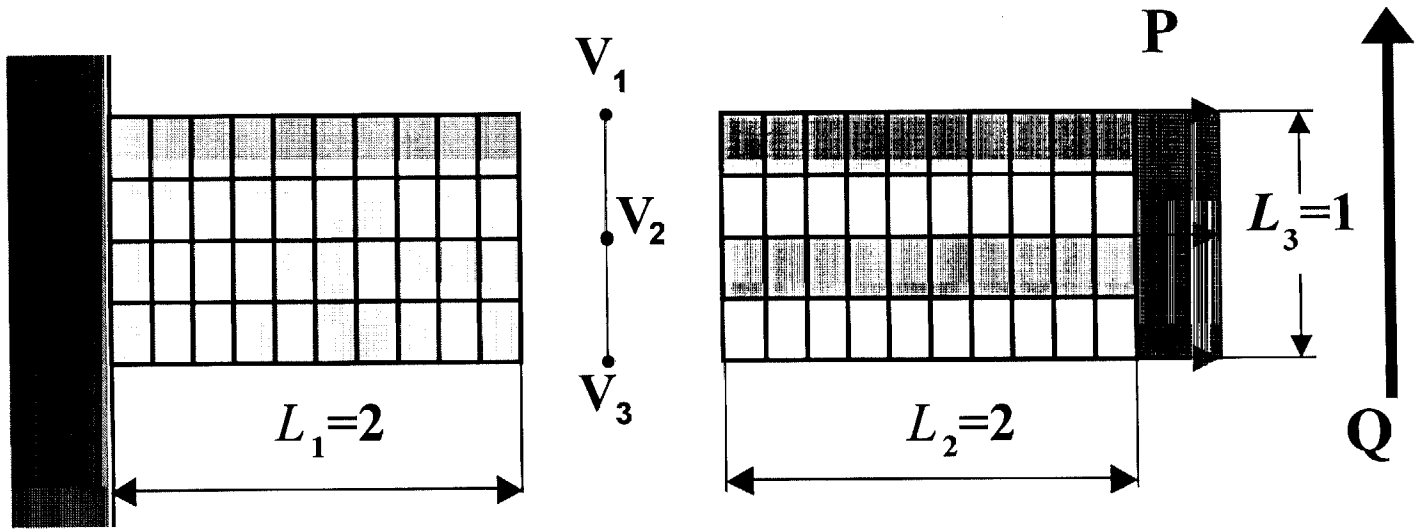

Figure 14. 2D- Composite cantilever beam with vertical interface.

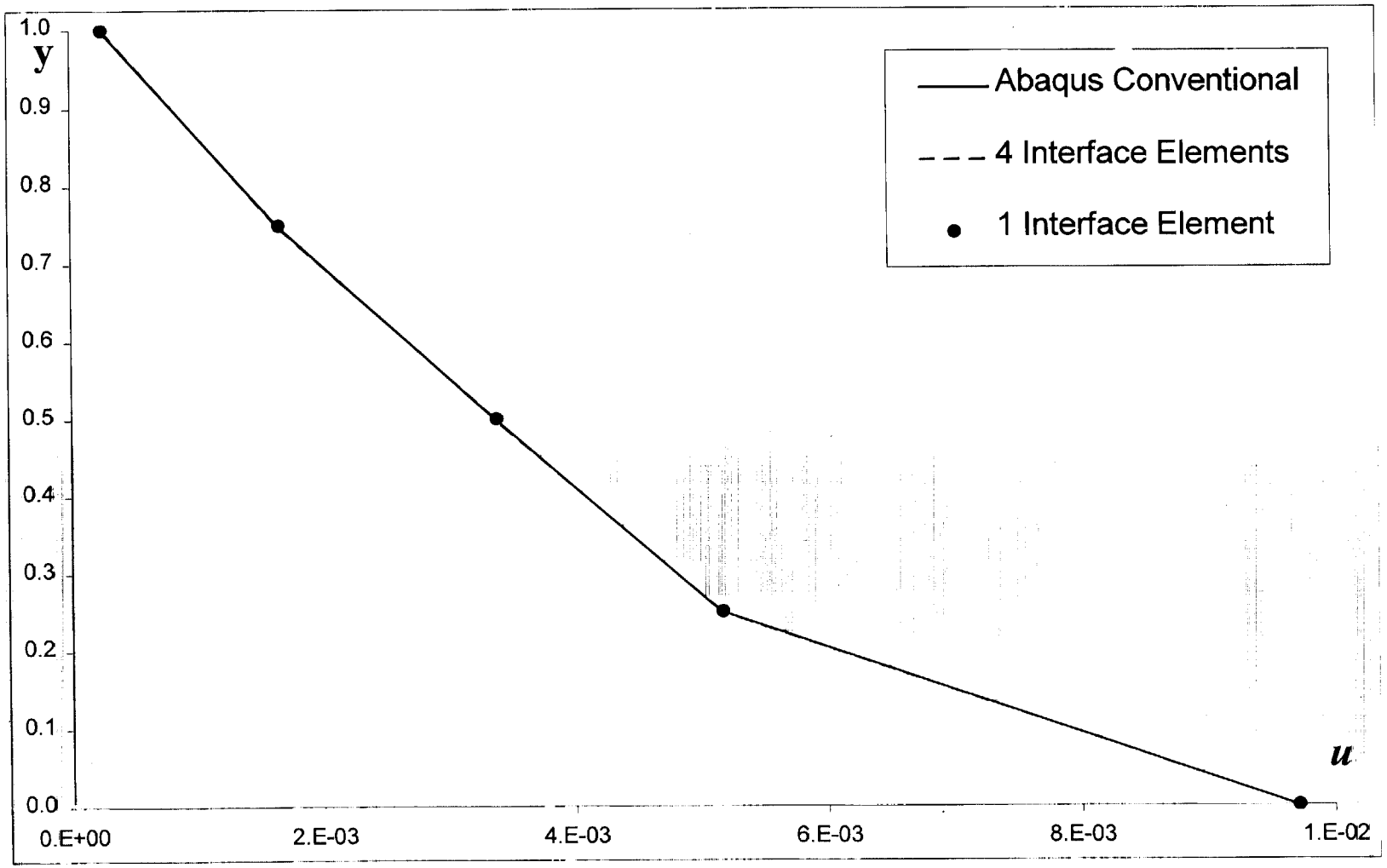

Figure 15. Beam extension along the thickness at the free end under axial load.

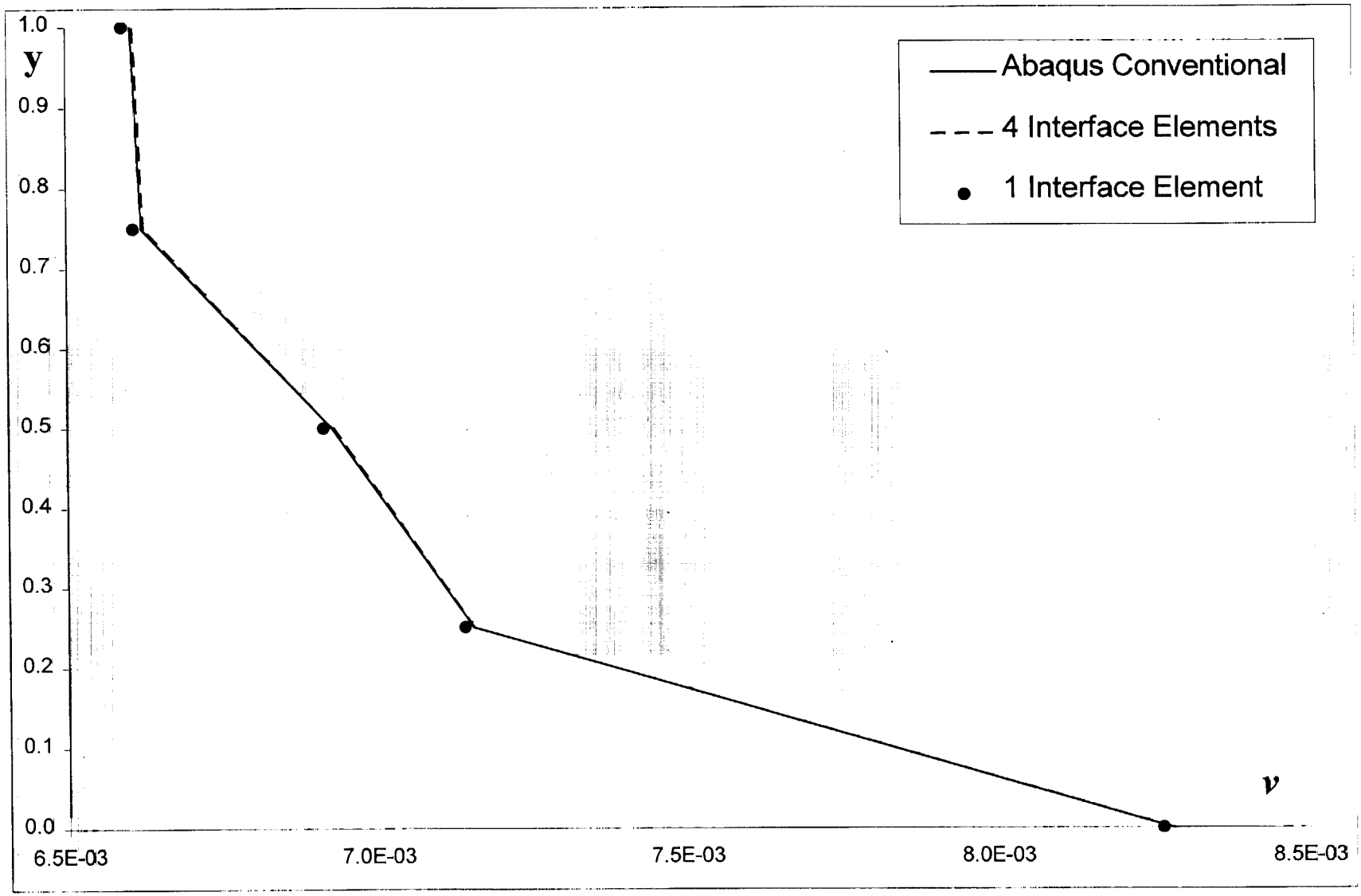

Figure 16. Beam vertical deflection along the thickness at the free end under axial load.

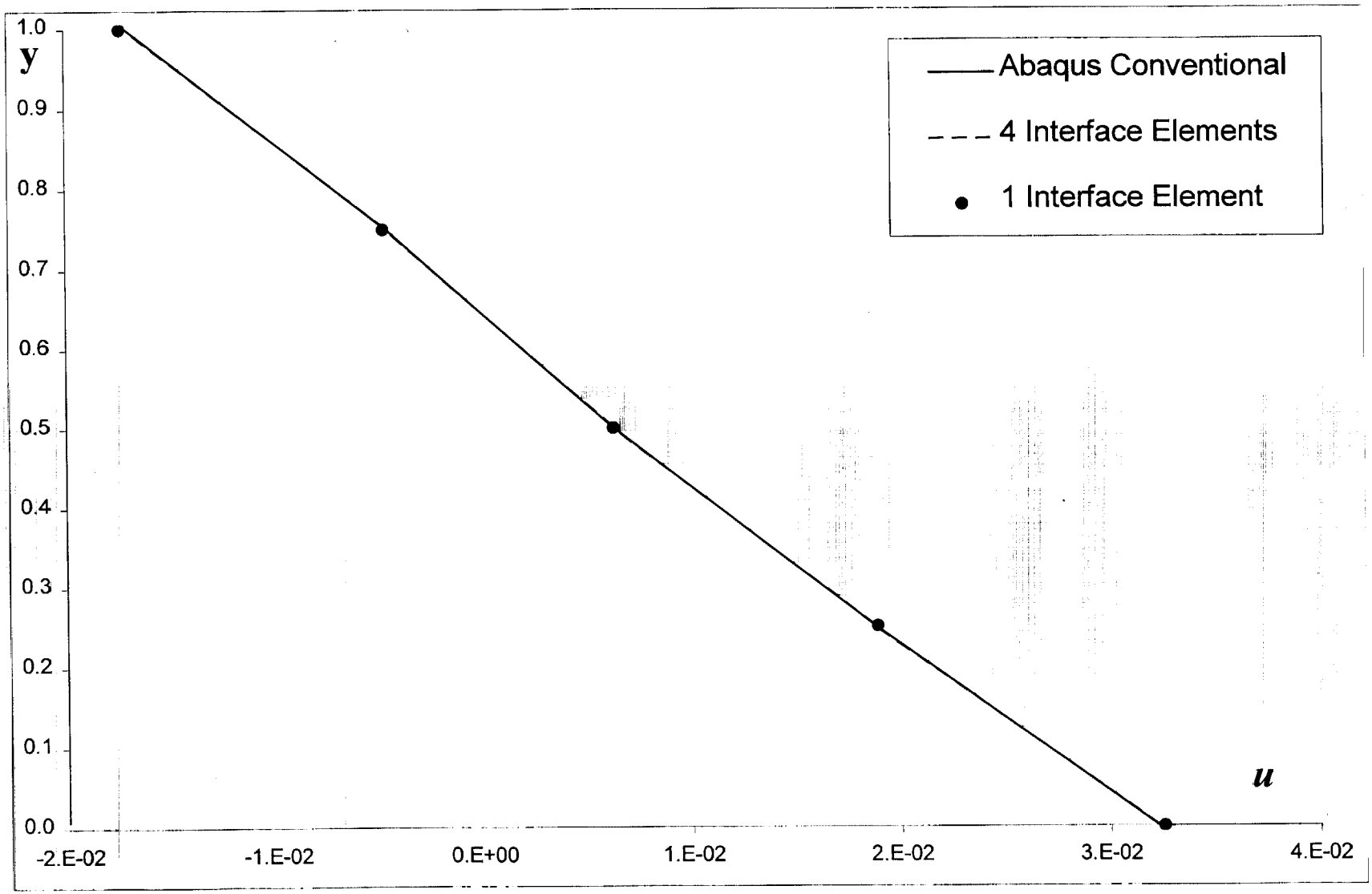

Figure 17. Beam extension along the thickness at the free end under transversal load.

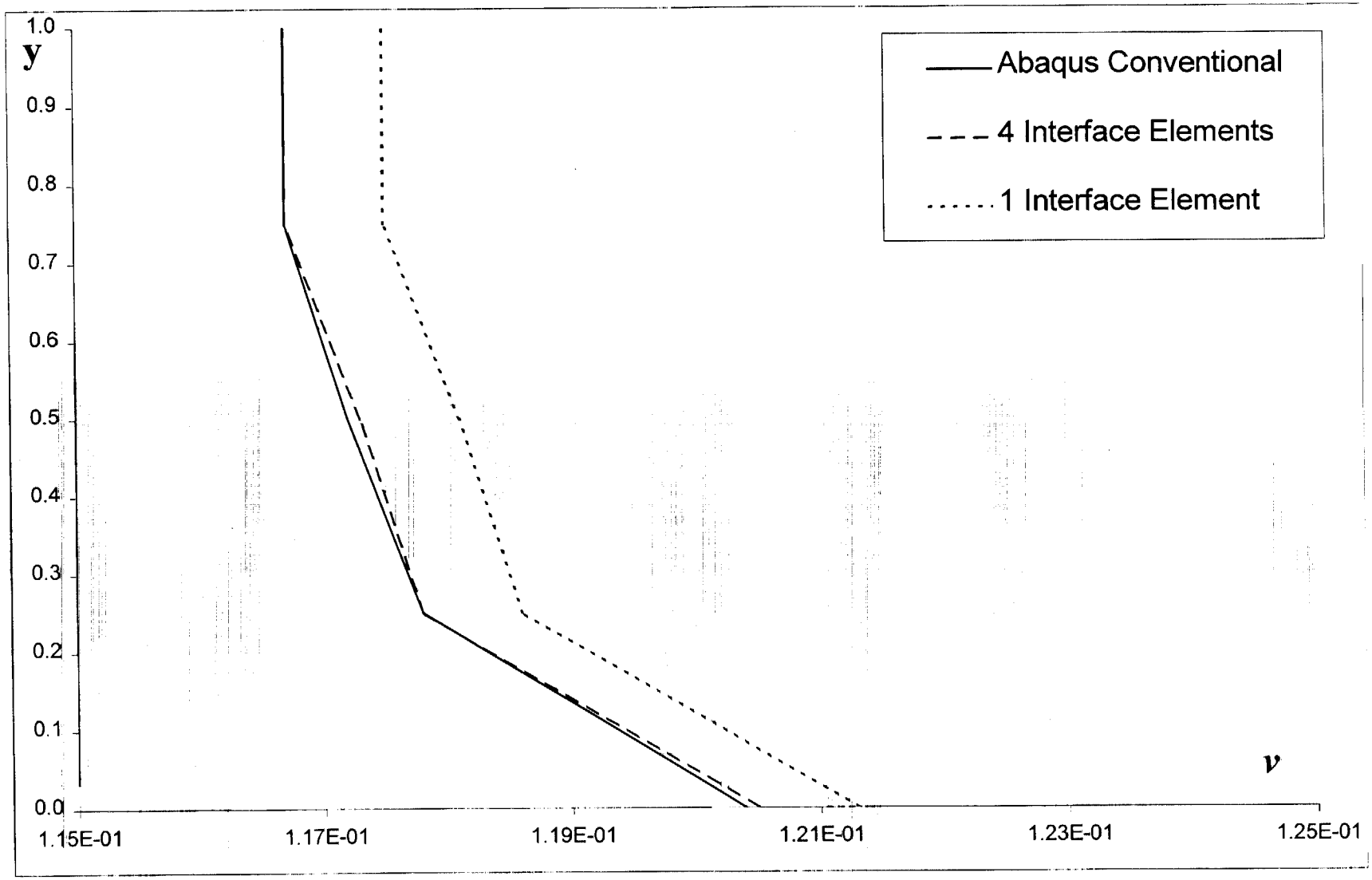

Figure 18. Beam vertical deflection along the thickness at the free end under transversal load.

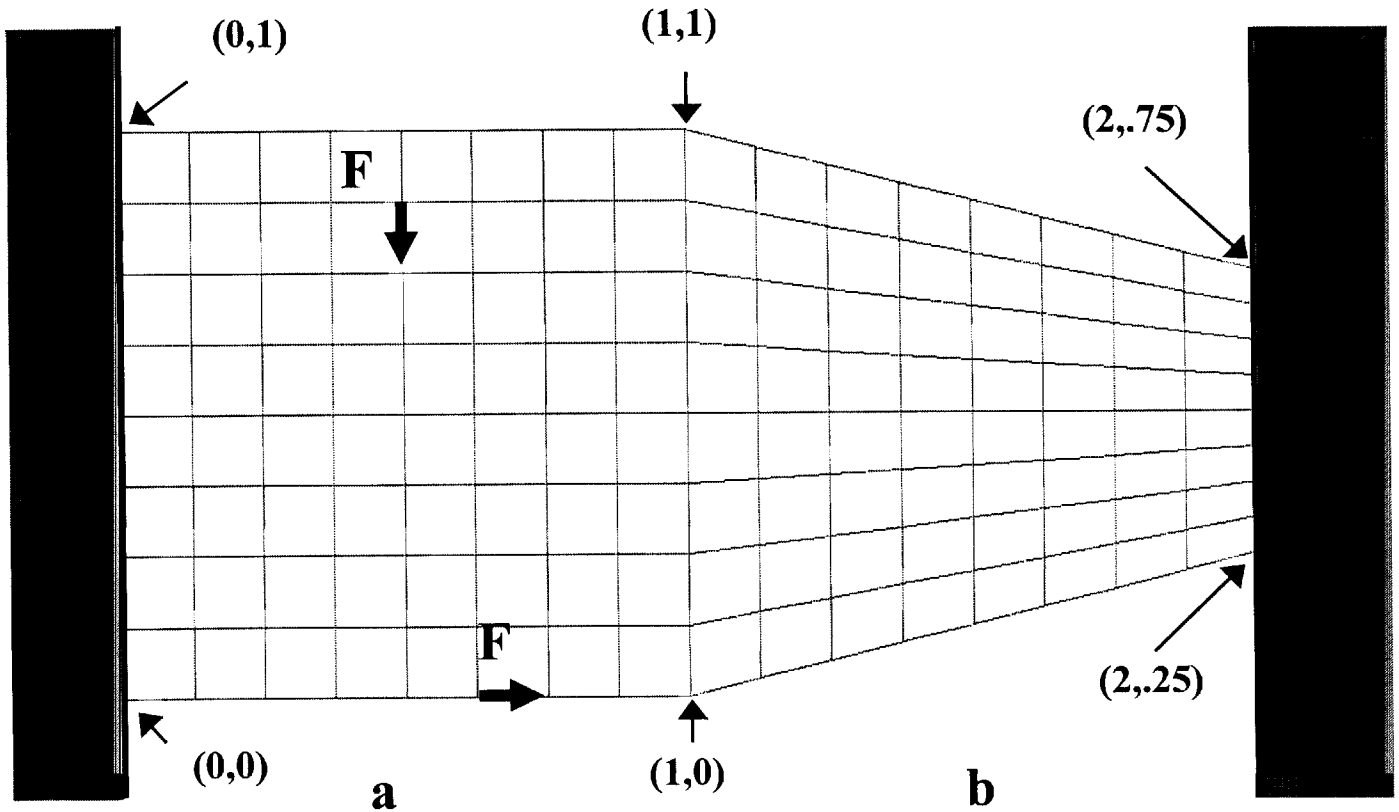

Figure 19. Clamped-clamped two-piece asymmetric beam. The data in parentheses represents the x and y coordinates of the point indicated.

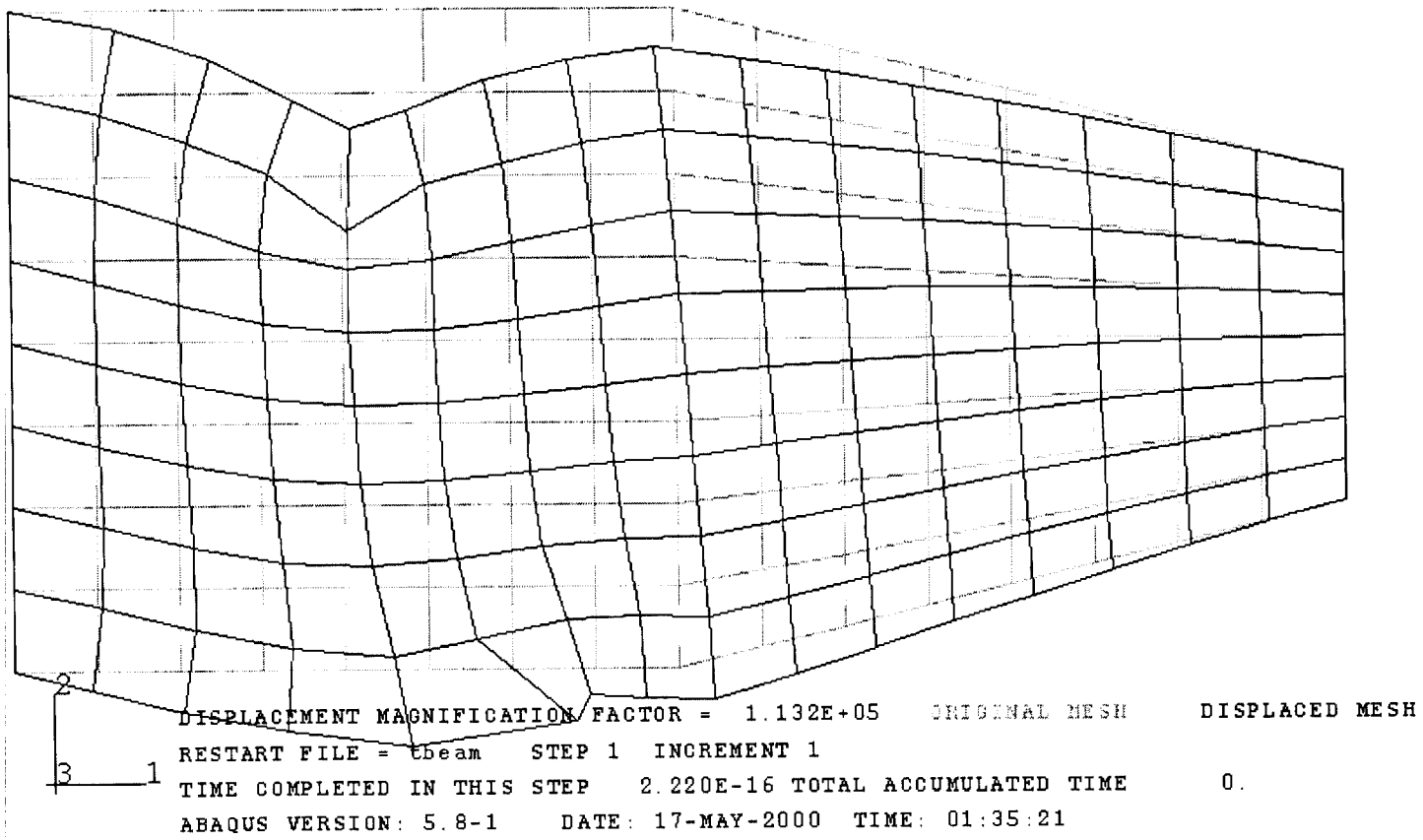

Figure 20. Deformed configuration obtained through conventional Abaqus FE solution.

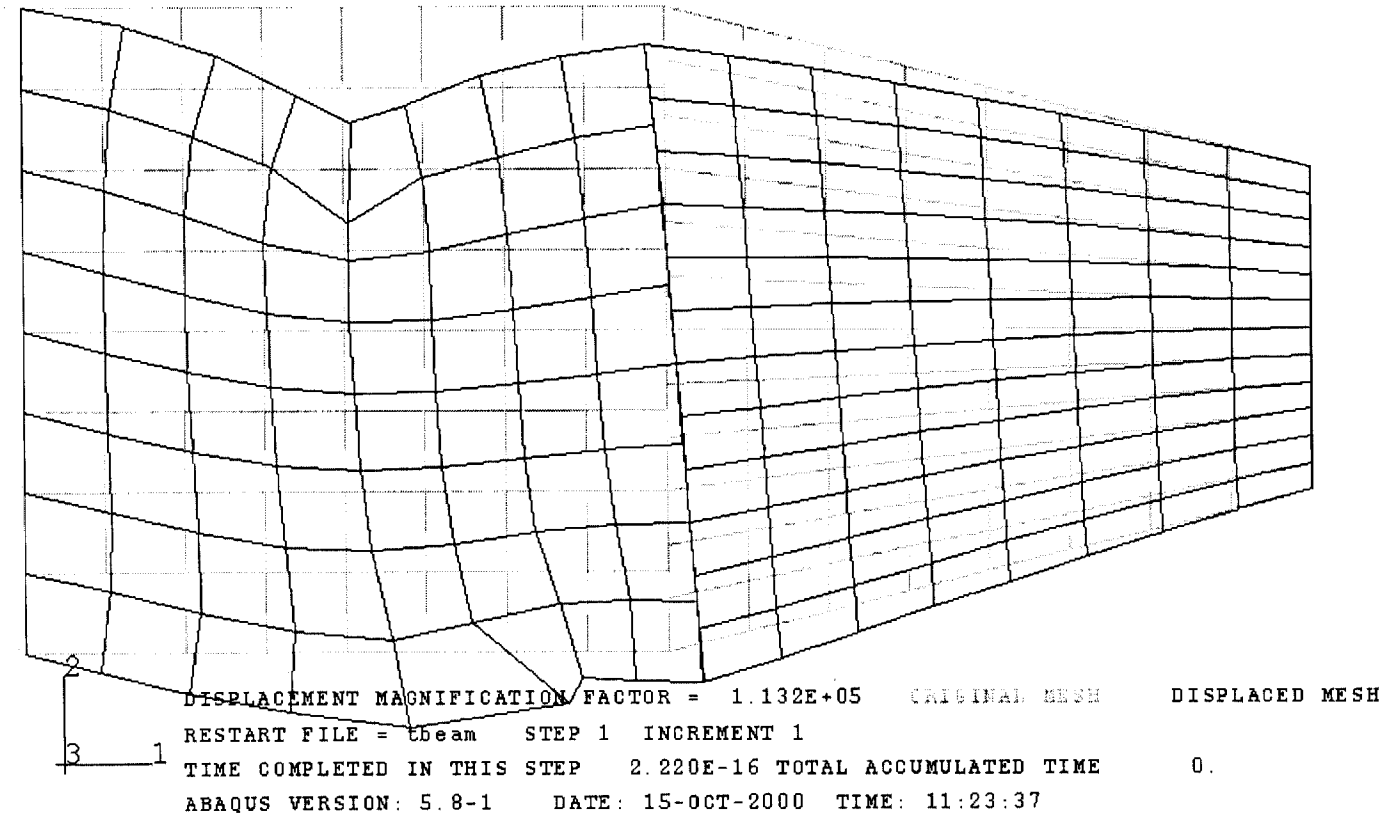

Figure 21. Deformed configuration obtained using interface elements approach.

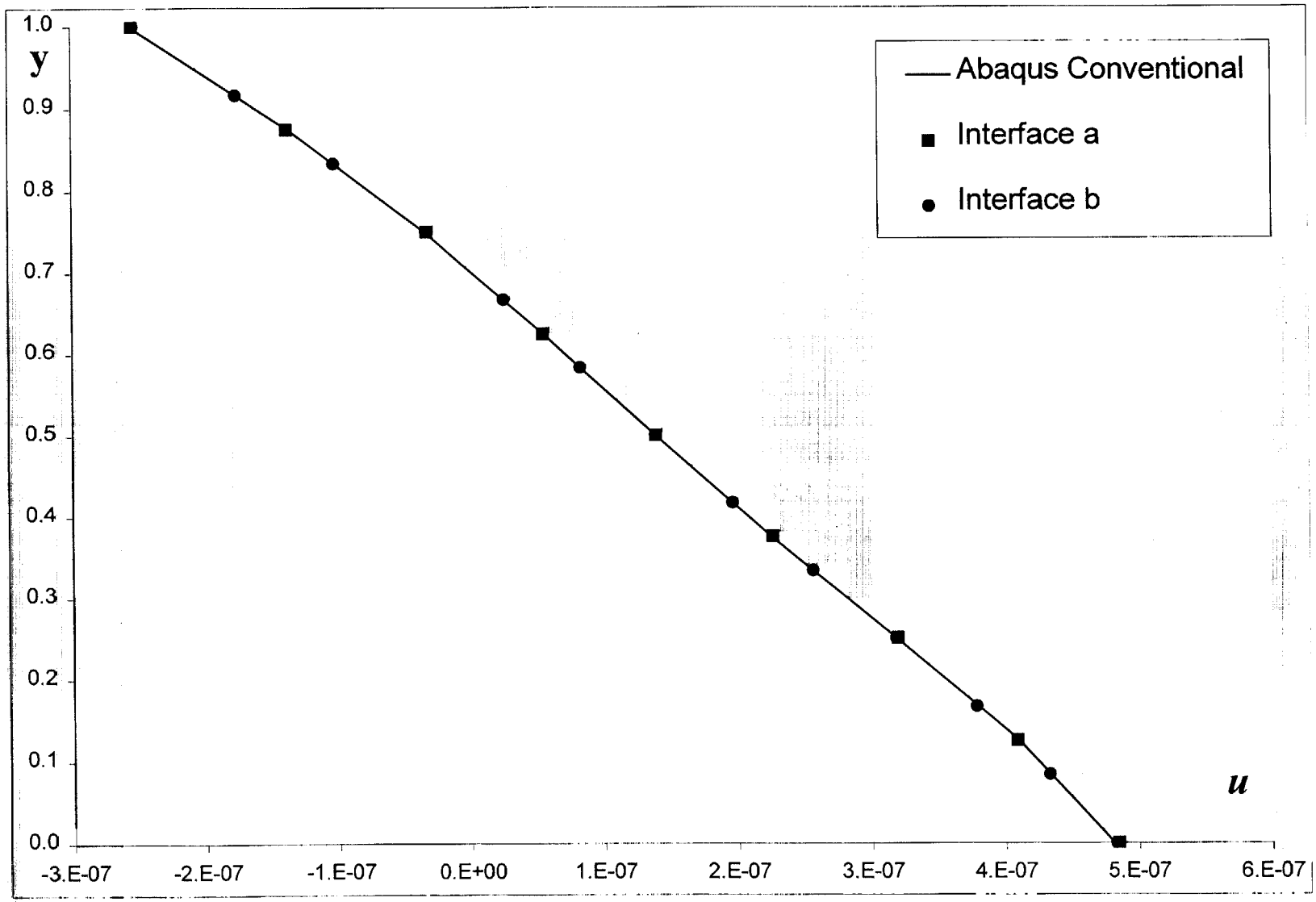

Figure 22. Axial displacements along the thickness at the interface.

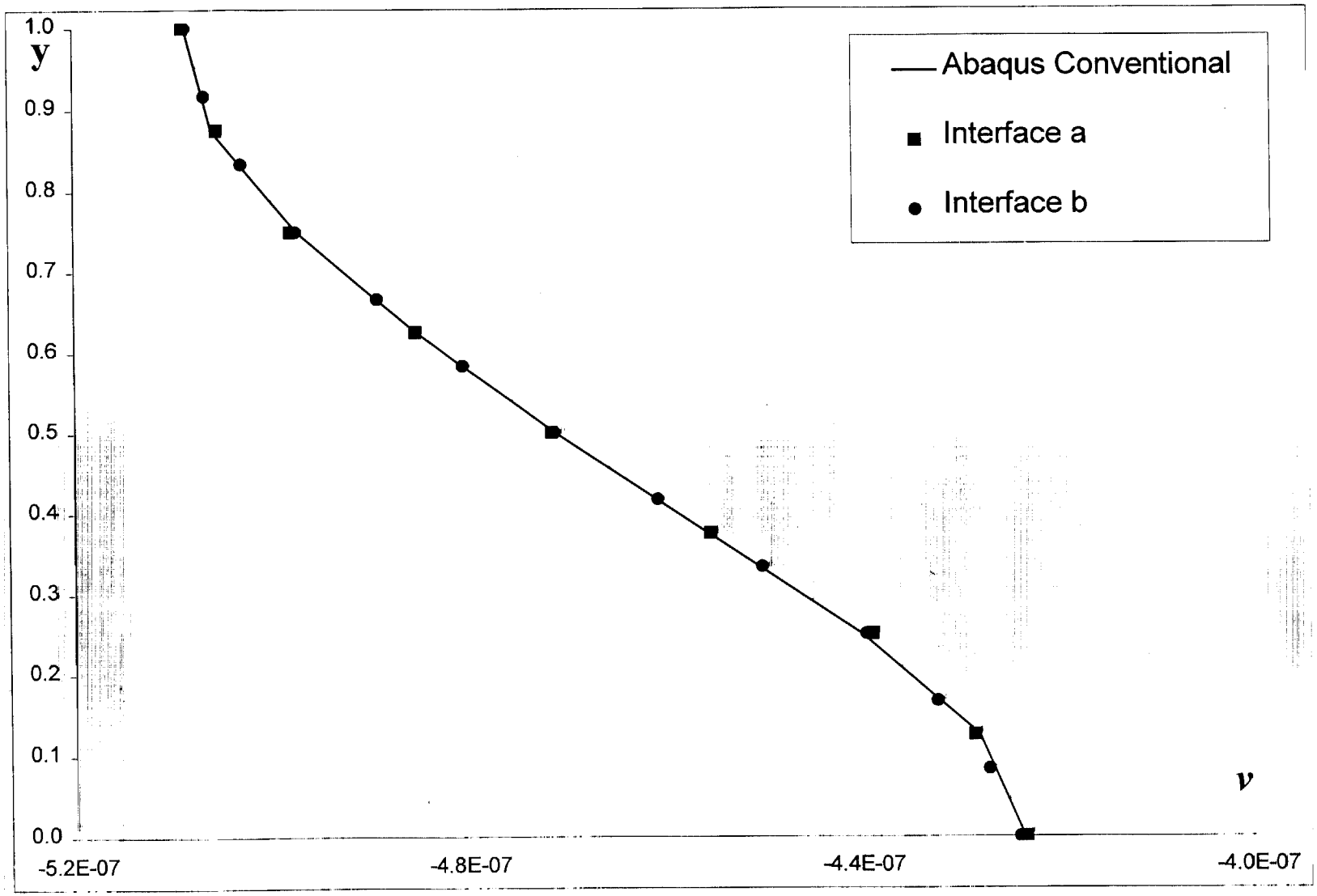

Figure 23. Transversal displacements along the thickness at the interface.

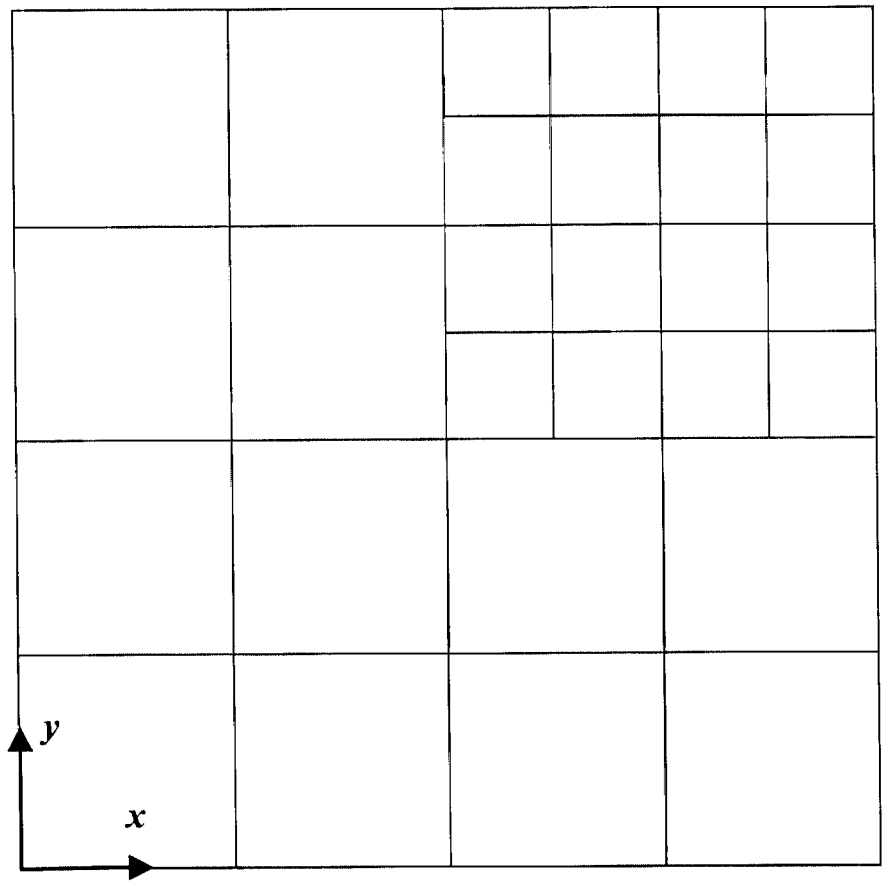

Figure 24. Penalty interface FE model of a flat plate.

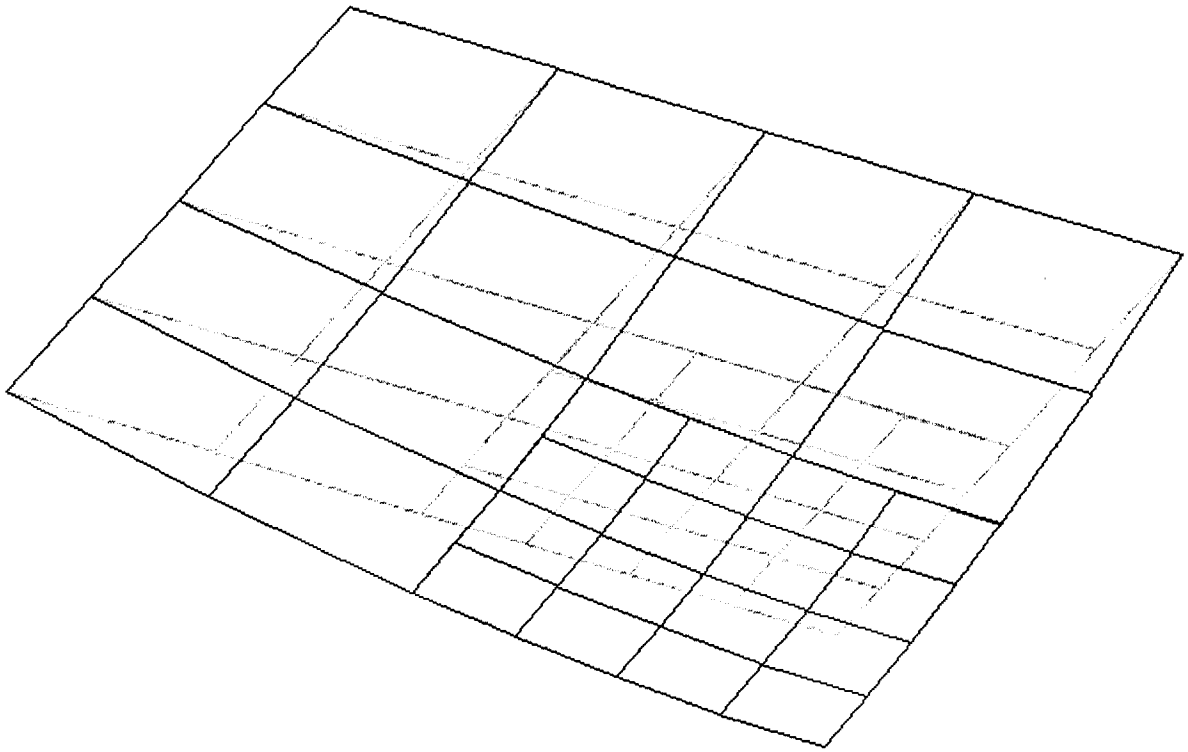

Figure 25. Original and deformed mesh as seen from the bottom of the plate.

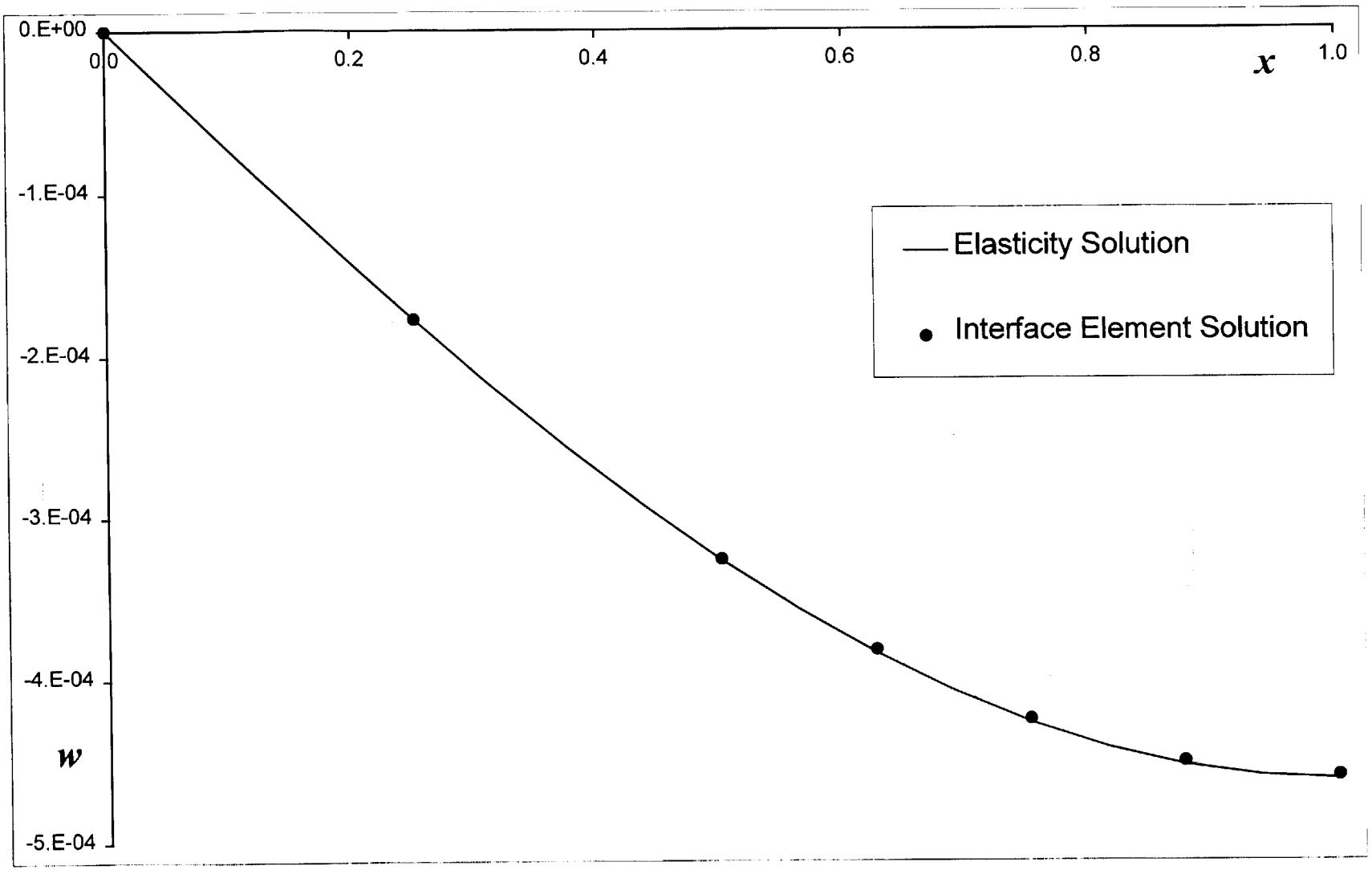

Figure 26. Variation of the transverse displacement w along x at $y = 1$.